Aerial Observations of the Yugoslavian Bora

RONALD B. SMITH

Yale University, New Haven, CT 06511

(Manuscript received 10 March 1986, in final form 14 July 1986)

ABSTRACT

The first aircraft observations of the bora in Yugoslavia were accomplished during the ALPEX project in 1982. Data from all five ALPEX bora flights have been analyzed in a comparative study of bora structure. Although the bora varies considerably in depth, in the strength of the incoming low level flow, and in the direction of the winds aloft, several common features are evident. These include: upstream descent and acceleration beginning where the mountains rise; an approximate coincidence between the depth of the uppermost descending streamline and the wind reversal level upstream (when a reversal exists); a decoupling of the flow aloft associated with a splitting of the inversion and the formation of a thick mixed layer downstream; a narrow region of intense turbulence and an ascending jet just downstream of the plunging bora. The bora structure is similar in many respects to the Boulder windstorm. Internal hydraulic theory, taking into account the decoupling effect of the intermediate layer, appears to describe both phenomena.

1. Introduction

One of the most famous local winds is the bora; a severe northeasterly wind coming down from the mountains along the Adriatic coast of Yugoslavia. A considerable amount is known about the climatology of this wind, and several clues to its dynamics have been found in surface and balloon observations (Yoshino, 1976; Jurčeč, 1981). Until the ALPEX program of 1982, however, no in situ aircraft observations of the bora had been carried out and thus several central questions concerning the generation of this wind have gone unanswered. As an example, the popular idea that the bora is a "fall wind" has not been verified. A fall wind would be defined as a wind which accelerates, due to its low temperature and greater density, as it moves downslope. The bora in fact has often been considered the prototype fall wind. Similar phenomena around the globe have been referred to as bora or bora-type winds (e.g., Reed 1981).

Beyond the interest in the bora as the "type" fall wind, there is the question whether it may have elements in common with other downslope winds; for example, the well-known Boulder windstorm (Lilly and Zipser, 1972; Lilly, 1978). The categorization of downslope winds has never been satisfactorily accomplished and certain features may be common to all. An understanding of the aerological structure of the bora may broaden our perspective and move us closer to a solution of this unsolved problem in atmospheric dynamics.

During the ALPEX Special Observing Period (SOP) of March and April 1982, four extended periods of bora occurred: 5–7 March, 21–25 March, 13–16 April, and 27–30 April. The length of these periods made it possible to schedule one or two research flights during three of them. On each of five days—6, 7, 22 and 25 March and 15 April—one or two aircraft probed the atmosphere above the Yugoslavian coast near Senj (Fig. 1). Climatologically, this region, and the region further north near Trieste, experience the strongest and most frequent bora windstorms.

The repeated research flights within the same bora period (6 and 7 March or 22 and 25 March) are not redundant as the bora slowly changes during the periods. Even flights on consecutive days (e.g., the 6 and 7 March flights) found quite different bora structures. Repetitive flights are essential to reveal the nature of these changes. The availability of five different datasets provides a minimum sample to gain a reasonable view of bora variability. Whether five is sufficient for this purpose is an open question.

An added factor is that the flight tracks for each research mission are different. Part of this is due to the change in preflight planning which occurred as the scientists and aircrews learned more about the phenomena and how to probe it thoroughly and safely. A second reason for the variability is the change in local flight regulations due to changes in cloudiness and local air and sea traffic. Just as no two boras were identical, no two research flights were identical. Table 1 summarizes the five bora situations and research flights.

The purpose of this report is to examine the similarities and differences between various bora cases. No detailed discussion of any particular bora event will be given. This work extends several preliminary reports of the ALPEX bora cases (Smith, 1982, 1984; Koracin, 1984; Vucetic, 1984; Jurčeč, 1984; Mahrt, 1984).

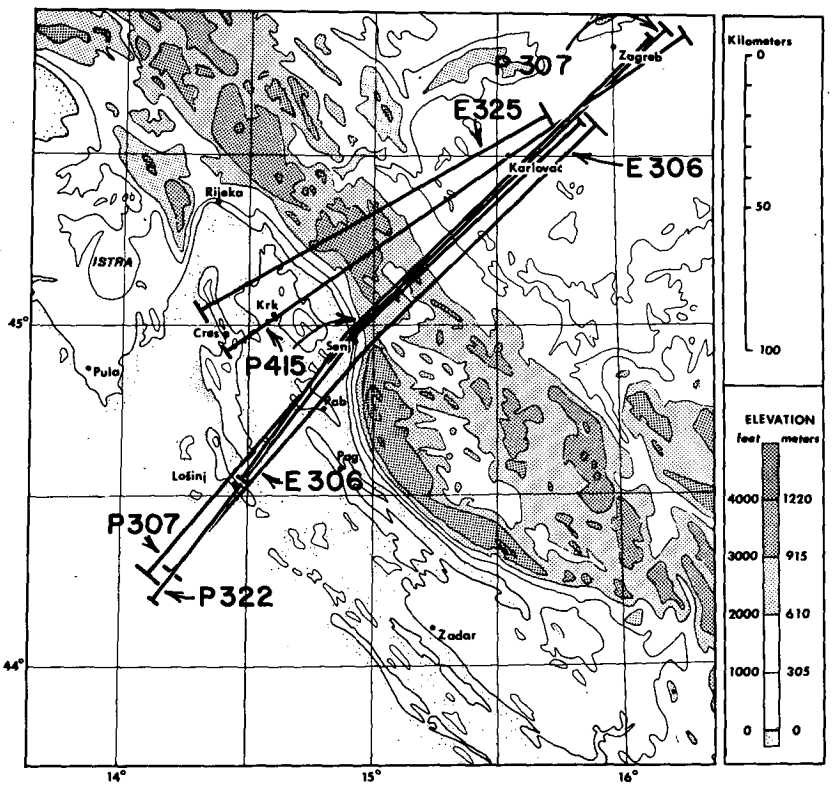

FIG. 1. The Dinaric Alps and the northeastern Adriatic Sea. Cross-section flight tracks for all five ALPEX bora missions are shown. Code (i.e., E306 = Electra 3/06/82) gives aircraft, month, and day. Error bar at end of track suggests lateral variation of track on repeated legs.

2. Bora periods

The longevity of the bora is one of its primary characteristics. A duration of four to six days is not unusual. Changes in atmospheric structure during three ALPEX bora periods are depicted in time-height diagrams in Figs. 2, 3 and 4. The station shown, Zagreb, is representative of the region northeast of the coastal range and is upstream in relation to the low level winds. The supply of cold air from the northeast is reflected in the inversion height and strength, and the wind speed at Zagreb at 900 mb and the surface. The 900 mb level is chosen as being above the surface layer but below the inversion in most cases. The strength of the bora is indicated both by the surface wind at Senj (the component from 60° from the north) and the sea level pressure difference between Zagreb and Senj. These measures fluctuate somewhat and generally weaken over a several day bora period.

The bora begins strongly with the arrival of low level cold air from the northeast. Figure 2 shows an example of this at 0300 UTC 5 March 1982. Over several days the cold air supply weakens both with respect to its depth, coldness and approach velocity. As the supply weakens, the bora at Senj diminishes only slightly, and finally ceases only when the supply is totally exhausted. In a sense, the most remarkable bora accelerations occur late in the period when the surface winds at Senj may still be 15 m s^{-1} while the 900 mb winds at Zagreb have dropped to 3 or 4 m s^{-1}.

Another important feature of the bora environment is the wind turning across the stable layer. It is not surprising that the wind turning tends to be concentrated in the stable layer, as that is where the horizontal pressure gradients can change rapidly with height; furthermore, larger wind shear can be accommodated there without shearing instability. As indicated in Table 1, almost all quadrants of upper-level wind direction are included in our sample of five cases. Only the 25 March case has northeasterly winds at all levels.

3. Bora cross sections

In order to directly compare the five boras, a common scheme of cross-sectional presentation has been adopted. Some bora missions included three-dimensional patterns as well but these will be described in a later section (4). For each cross section flown by the ALPEX research aircraft, four panels are shown: (a) horizontal wind field; (b) potential temperature; (c) a moisture variable (liquid water, dewpoint depression, or mixing ratio depending on conditions); and (d) turbulence intensity taken as the vertical velocity variance. The one exception to this is 25 March where the mois-

TABLE 1. Alpex bora flights.

	Date				
	March 6	March 7	March 22	March 25	April 15
Approach of bora air	Strong from NE (inertial circle around eastern Alps)	Moderate from ENE	Strong from E	Weak from NE	Weak from NE
Zagreb winds (60° component at 900 mb)	16 m s^{-1}	12 m s^{-1}	14 m s^{-1}	4 m s^{-1}	7 m s^{-1}
Approximate depth of bora	3.5 km	2.2 km	3.6 km	2.2 km	2.2 km
Senj winds (Dir. = 60°)	24–20 m s^{-1}	19–23 m s^{-1}	18–12 m s^{-1}	16–12 m s^{-1}	18–17 m s^{-1}
ΔP Zagreb–Senj	8–6 mb	5–6 mb	5–4 mb	2–3 mb	6–5 mb
Winds aloft	SE	SE	NW	NE	SW
Clouds	Heavy stratus cloud with measurable liquid water, clear window	Solid stratus upstream of mtn. crest, roll cloud (Plates 1–6)	Scattered	Clear with upper level wave cloud (Plates 7–8)	Dissipating stratus upstream of mountain crest; roll cloud (Plates 9–10)
Flight designation	E306 F306	P307 F307	P322	E325	P415
Flight track	Senj section only	Senj section only	Senj section and cross legs	Krk section	Senj and Krk sections, and small scale box pattern around Krk

ture field contained little information and is therefore not presented. All cross sections lie generally northeast to southwest. The track is variable from case to case (see Fig. 1) but the northeast end is always close to Zagreb so that the data there can be compared with the Zagreb time–height sections in Figs. 2, 3 and 4. The Zagreb and Karlovac soundings are included on each cross-section.

a. 6 March

The first ALPEX bora flight occurred during midday on 6 March 1982, about 30 hours after the onset of the bora period (Fig. 2). This bora case was relatively deep and moist. As shown in Fig. 5a, the northeasterly flow extended to nearly 3.5 km above sea level and included a thick stratus cloud (Fig. 5c). Below the cloud, air was extremely dry with the dewpoint depression dd = 12°C. From the θ_e isentropes slight lifting was evident northeast of the ridge in the lower parts of the cloud, with descent aloft. Droplet evaporation occurred soon after general descent began, forming a window in the cloud layer. This observation is consistent with the observed liquid water content 0.1 ± .05 gm m^{-3} as such air could only sustain about 100 meters of descent before clearing. The incoming air, at 3.5 km for example, descended at least 1 km based on the θ_e curves (Fig. 5b). Only the air below 3.8 km descended strongly, with relatively undisturbed flow above.

Southwest of Senj the airflow was southeasterly at all levels measured. The region of constant equivalent potential temperature from 2.5 to 3.5 km was saturated and thus well mixed. This was consistent with the observed turbulent zones (Fig. 5d).

The lowest leg flown, $z \sim 2.3$ km, was clearly within the bora layer upstream. Acceleration was evident (Fig. 5a) from 45 kt (22 m s^{-1}) upstream to 60 kt (30 m s^{-1}) over the mountain crest. Further acceleration was not observed as the bora layer thinned and descended below the aircraft level. The upstream acceleration was presumably due to the favorable pressure gradient associated with descent aloft. The acceleration was also qualitatively consistent with the decrease in streamline spacing seen in Fig. 5b.

In Fig. 5a, air above and to the left of the 105° line (45° from the nominal 60° wind direction of the bora) was moving primarily into the section from the southeast. This is a potential source of confusion in these diagrams. For the southeasterly air above the bora, the station Zadar (see Fig. 1) would be a better upstream sounding but this data has not been used in the present analysis.

Systematic vertical velocities determined directly from the aircraft inertial platform and wind sensors are shown in Fig. 5c. Ten second averages of w are plotted and analyzed by eye. Regions with more than three values in rough agreement and support from other legs are considered to have a systematic vertical velocity. Two main features are evident: 1) a downdraft

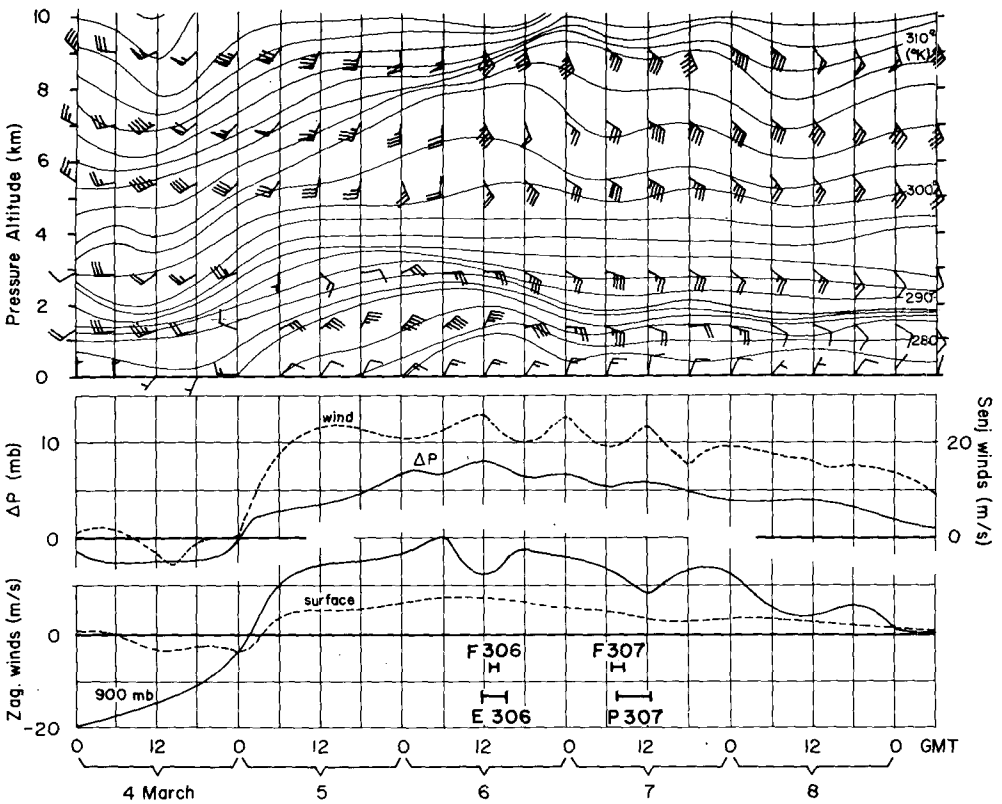

FIG. 2. Record of bora period from 4 to 8 March 1982. Upper panel: time–height section of potential temperature and wind derived from 6-hourly soundings from Zagreb. Middle panel: surface wind component (60°) at Senj and pressure difference between Zagreb and Senj. These are both measures of bora strength. Lower panel: 900 mb and surface winds at Zagreb. Duration of bora research flights are shown. Note the onset of bora with cold airmass arrival at 0300 UTC 5 March; the wind turning above NE bora flow; and the time evolution of inversion strength and height and bora depth.

directly over the mountain peak ($w = -3$ m s^{-1}) and 2) an updraft found at all levels ($w \approx 4$ m s^{-1}). The downdraft occurs in the northeasterly air and is consistent with the descending isentropes. The updraft occurred at the leading edge of the dense downstream cloud. Numerous other regions of vertical motion were present but are not shown because they were of small horizontal scale or magnitude or were encountered on one flight level only.

Strong turbulence was found just southwest of the main updraft and inside the cloud. Turbulence was strongest at the lowest flight level (2.3 km) but was still detectable at 4.7 km in the cloud. The variances shown in Fig. 5d are computed from one-second data according to

$$\left.\begin{aligned}\sigma_w &= \frac{1}{N}\sum_{i=1}^{N}(w_i - \bar{w})^2 \\ \bar{w} &= \frac{1}{N}\sum_{i=1}^{N} w_i\end{aligned}\right\}$$

for 10 seconds of flight ($N = 10$). With an aircraft ground speed of 126 m s^{-1}, this is an averaging length of 1.26 kilometers. In such an inhomogeneous field with a moving instrument platform, no precise separation between systematic velocities and turbulence is possible.

b. 7 March

Figure 6 shows the bora structure on the morning of 7 March. Almost all winds encountered by the aircraft were southeasterly, indicating that the aircraft was never really inside the bora air. This is consistent with the marked drop in the inversion and thinning of the bora layer observed during the previous 24 hours at Zagreb (Fig. 2). The aircraft could not descend lower due to control and safety restrictions on flight operations. Because of this, no direct evidence of bora acceleration could be obtained. Only a rapid downwind descent over Senj (1019 UTC in Fig. 6a) made possible a brief partial penetration of the descending air.

The upstream soundings from Karlovac and Zagreb indicated a stable shallow bora flow from the northeast. The precise pattern of isentrope descent could not be determined, but the final drop over Rab must have

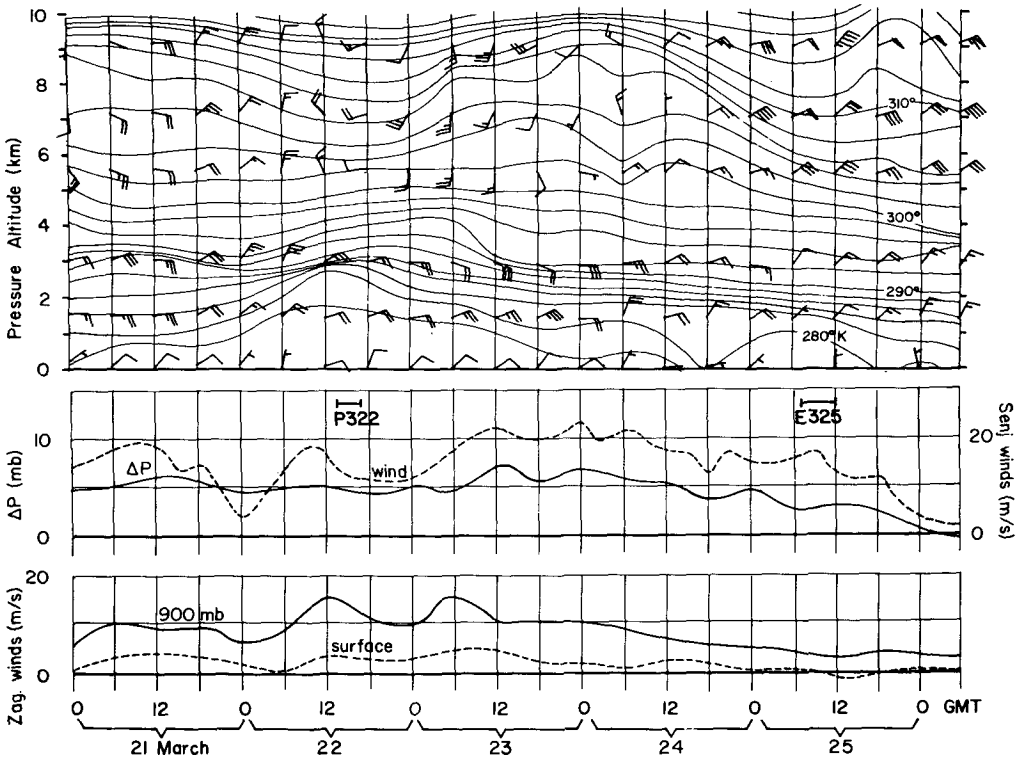

FIG. 3. As in Fig. 2 but for bora period from 21 to 25 March 1982. Weak bora began before the period shown. Note change in midtroposphere wind direction (W to N to S, to NE) during period. Bora continues until 1800 UTC 25 March in spite of weak approaching flow at Zagreb.

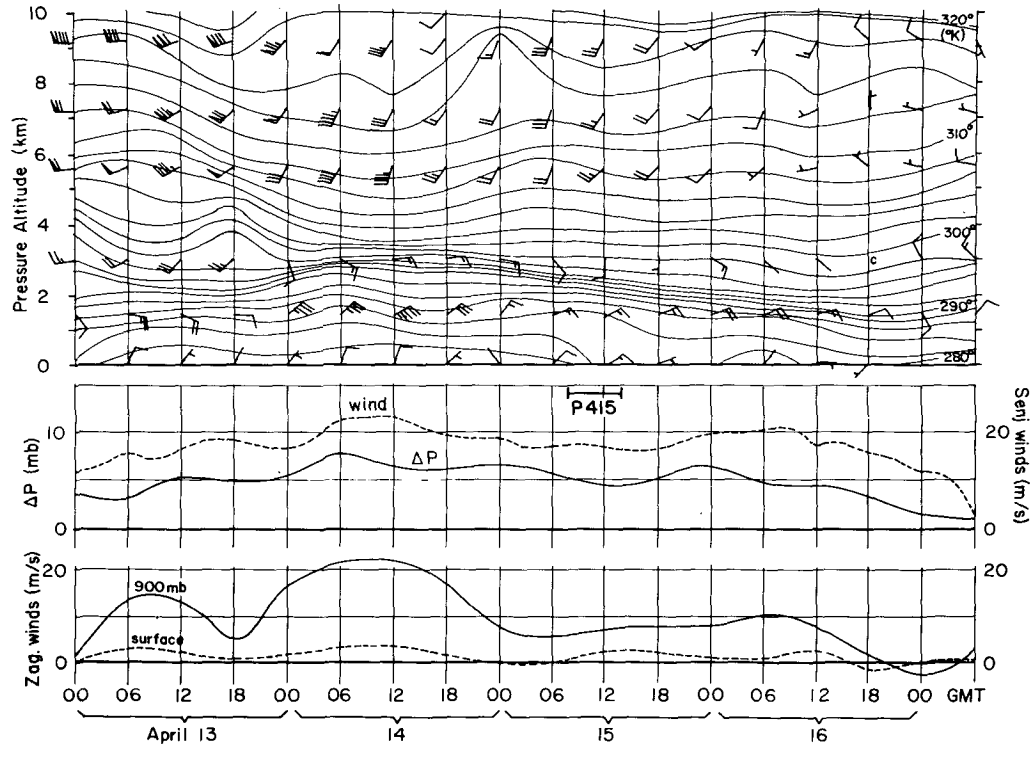

FIG. 4. As in Fig. 2 but for bora period 13–16 April 1982. Note deep strong bora on the 14th changing to somewhat shallower and weaker flow on the day of mission P415.

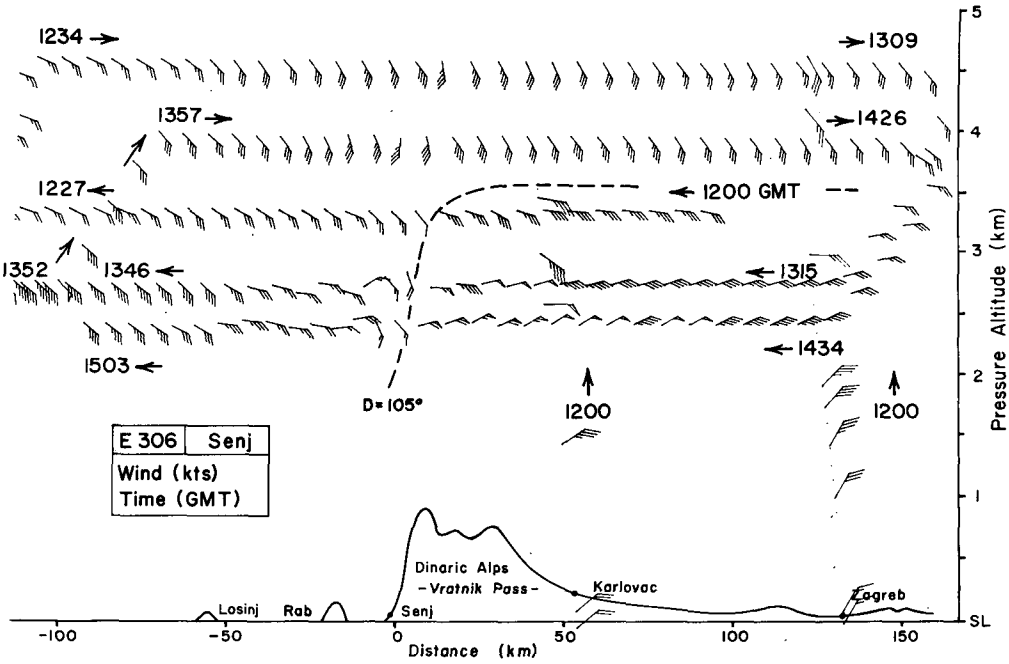

FIG. 5a. Wind cross section for mission E306, from aircraft data and sounding at Karlovac and Zagreb. Section includes horizontal wind (as standard barbs) and topography from radar altimeter. Dashed line (direction = 105°) indicates where wind direction has turned 45° from the bora wind direction (nominally 60°) and roughly defines the region of bora wind. Depth of bora allowed several traverses within the NE air. These legs reveal an acceleration of the bora air from 45 kt (23 m s^{-1}) to 60 kt (32 m s^{-1}) upstream of the ridge crest. Observation times are given in UTC. Vertical exaggeration is 37:1.

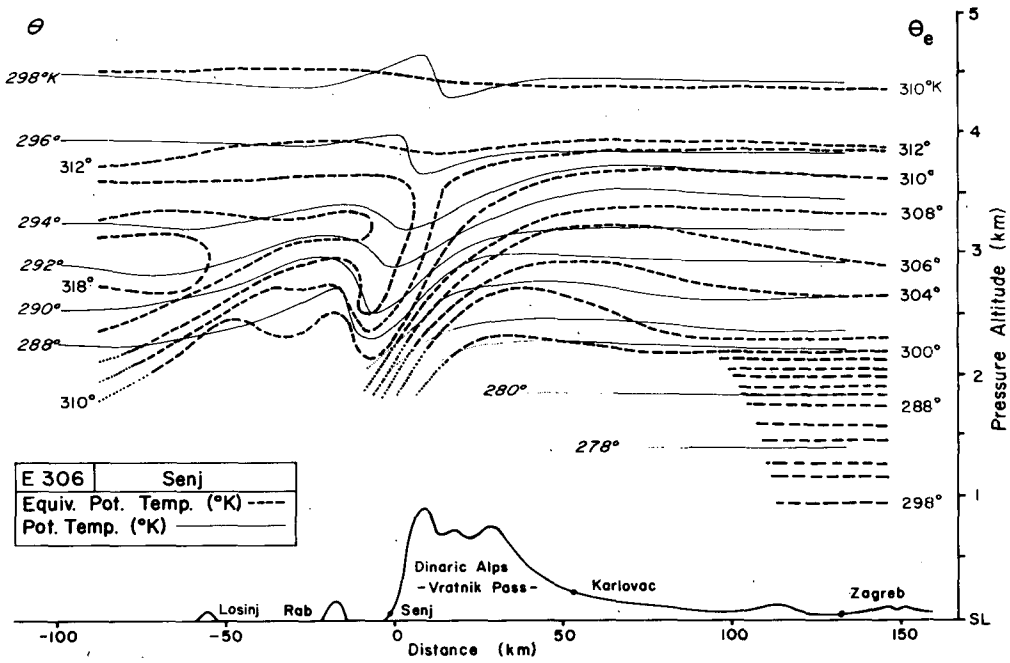

FIG. 5b. Potential temperature cross section for E306. Solid lines (dry θ) and dashed lines (equivalent θ) suggest the presence of strong descent below 3.5 km starting over Karlovac.

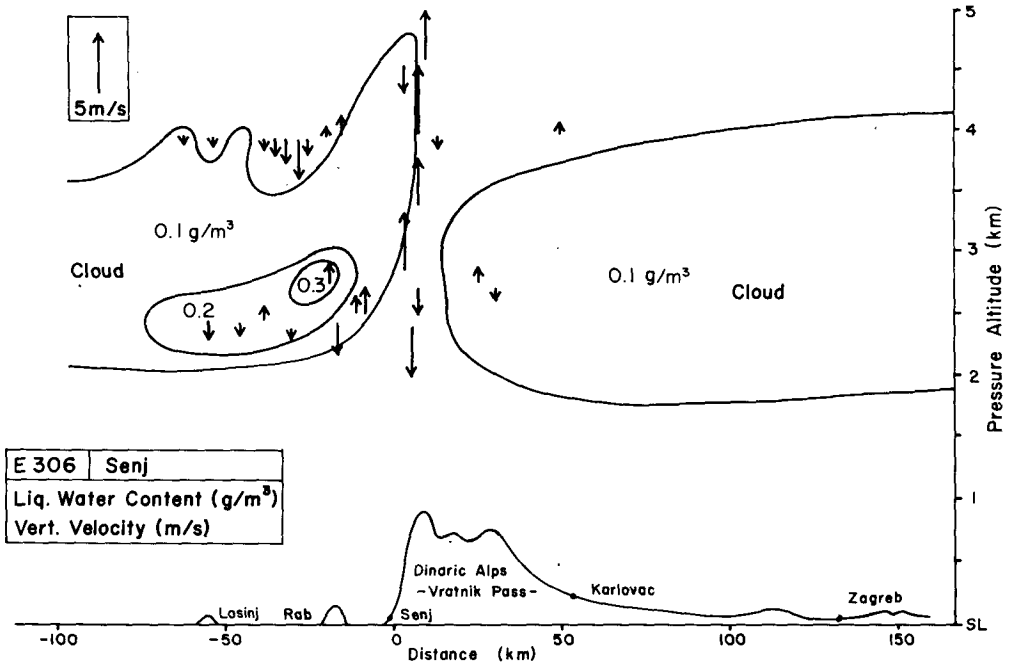

FIG. 5c. Liquid water cross section for E306. Descent of air downstream of the ridge crest produces a clear region followed by a dense lee side cloud. Vertical arrows indicate regions of systematic vertical air motion (i.e. persistent along ~2 km of flight track) derived from onboard air motion sensors. Strong descent (w approximately -4 m s^{-1}) over mountain crest is followed by strong updraft ($w \sim 4$ m s^{-1}) further aloft near edge of lee side cloud.

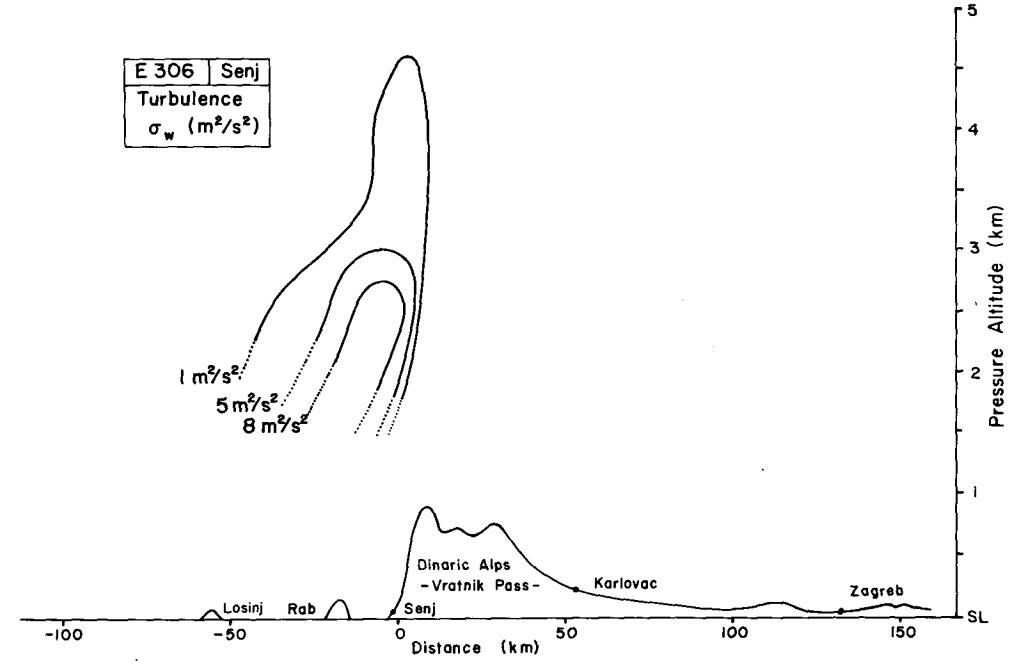

FIG. 5d. Turbulence cross-section for E306. Vertical velocity variance over 10 sec (~1300 m) of the flight track is shown, with no trend removal. Leeside turbulent region has a width of ~40 km and a depth of 2 to 3 km.

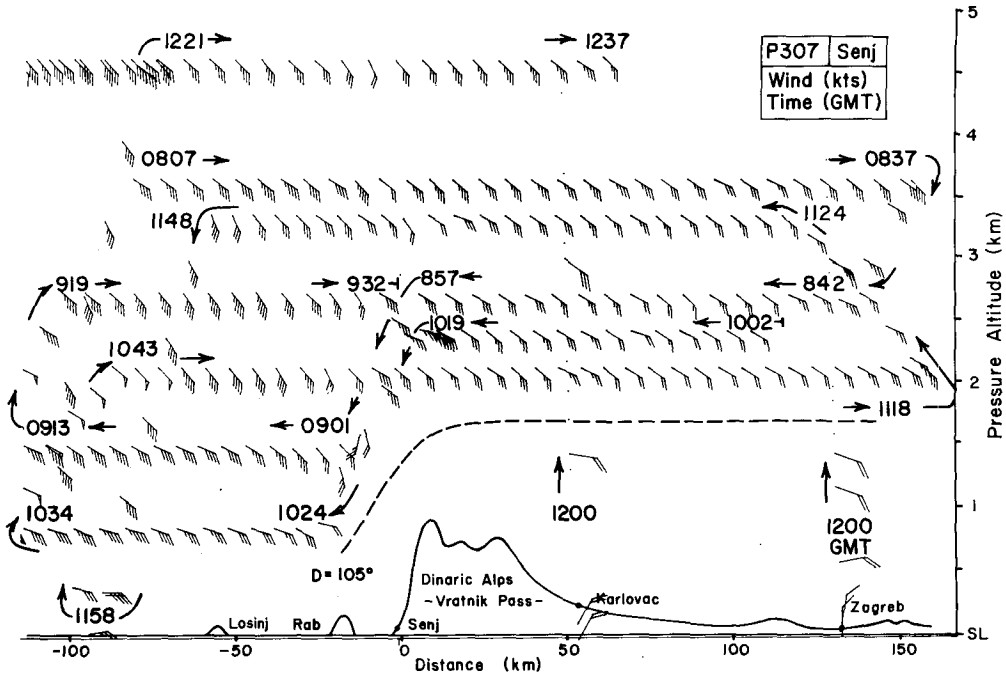

FIG. 6a. Wind cross section for mission P307. Shallowness of bora layer and obscuring clouds restricted aircraft penetration into bora layer.

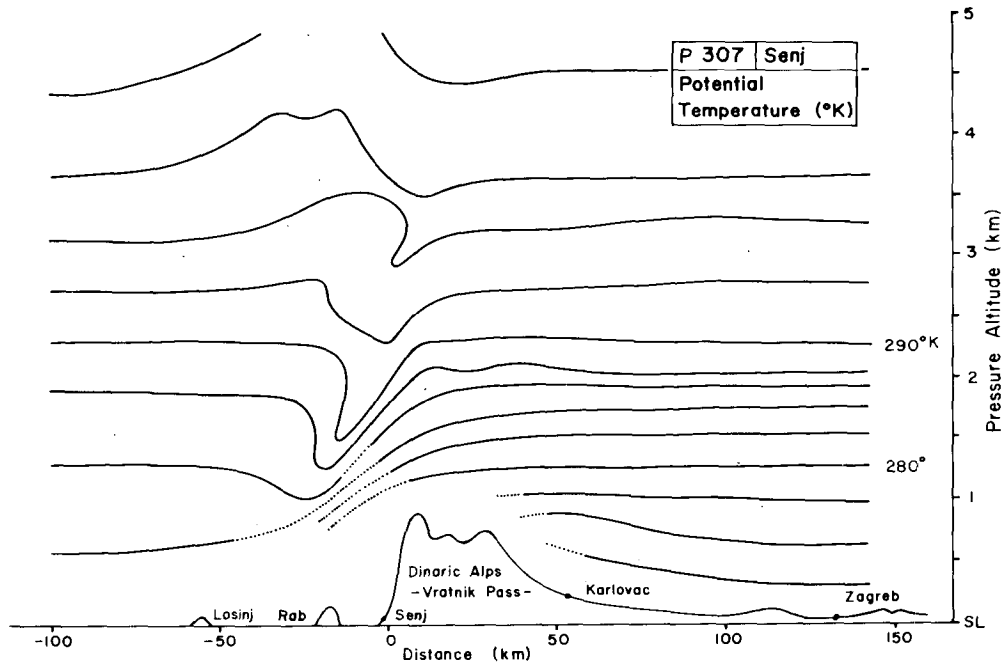

FIG. 6b. Potential temperature cross section for P307. Strong descent is evident below 2 km. Isentrope deflection aloft is in SE air (normal to section). Liquid water content is small enough that θ_e contours (not shown) are very similar to those shown. Lower troposphere is much less stable downstream of Rab, than upstream of Karlovac.

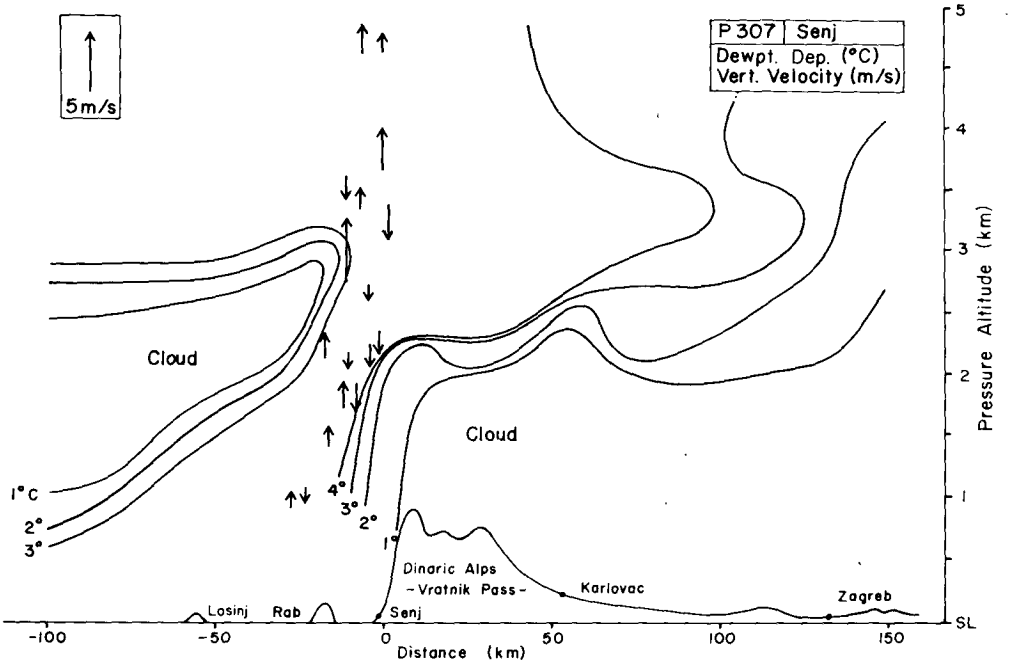

FIG. 6c. Dewpoint depression cross section for P307. Cloudy bora layer below 2.5 km clears in descent over the ridge crest, followed by leeside cloud reaching to 3.2 km. See Plates 1–6 for photographs of these clouds. In the vertical velocity field, ($w \sim 2$ m s^{-1}) is followed by ascent ($w \sim 3$ m s^{-1}) extending to 5 km.

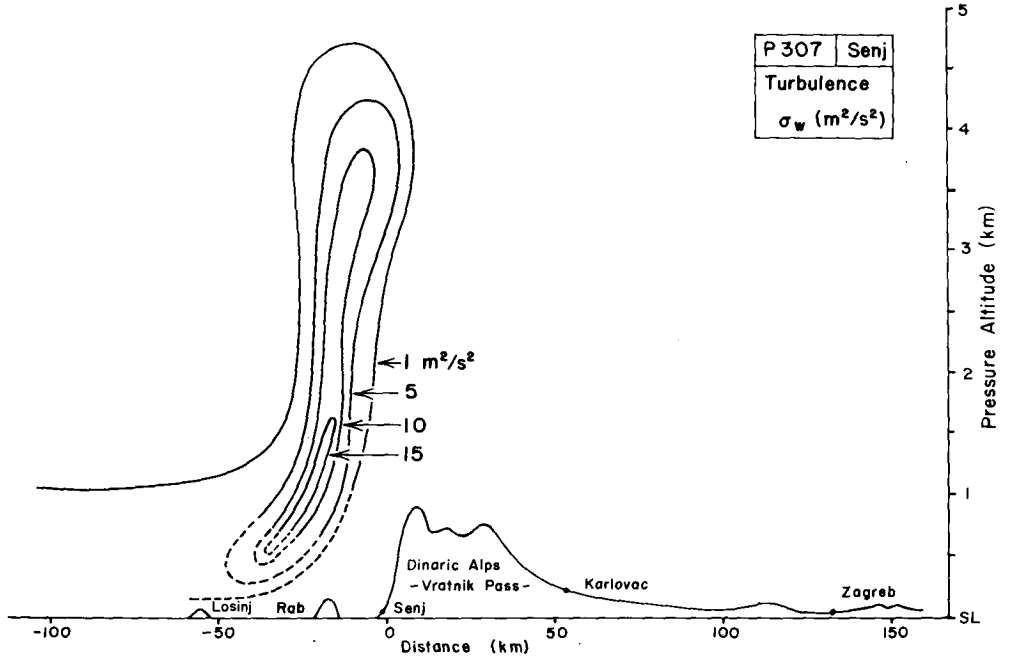

FIG. 6d. Turbulence cross section for P307. Intense region of turbulence has width of about 20 km and depth of about 4 km.

PLATE 1. View from Falcon (F307) at about 0800 UTC. View is SE past southern tip of Rab. Note clearing of bora stratus layer as it descends. No turbulent lee cloud is present along this section of the coast. Stratus over mountain crest is corrugated with rolls parallel to the wind below—and therefore with the wind shear, associated with the bora acceleration. (Photo H. Fimpel)

PLATE 3. View from P-3 (P307) at 0903 UTC at 44.7°N, 014.48°E. View is eastward past northern tip of Pag and the southern tip of Rab to the Yugoslavian coast south of Senj. Note clearing by descent and cloud lineation. (Photo A. Walker)

PLATE 2. View from the P-3 (P307) at 0745 UTC at 45.08°N, 015.03°E. View is south along the coast south of Senj. Note turbulent lee cloud extending part way to the south, and streamwise lineation in clouds over the crest, just before they disappear due to descent. (Photo A. Walker)

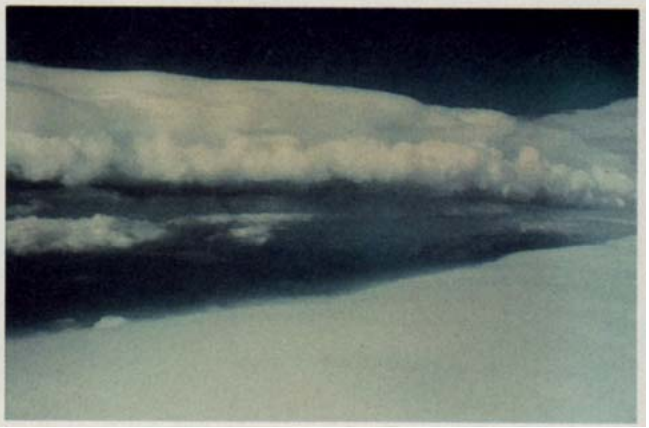

PLATE 4. View from P-3 (P307) at 0935 UTC at 45.05°N, 014.96°E. View is westward from a point over the mountains and bora stratus layer. Istra is visible below the turbulent lee cloud. Note smooth upper regions of the lee cloud. (Photo A. Walker)

reached 1 km. Deflected isentropes aloft and wind barb perturbations indicated a narrow zone of disturbance over Senj reaching to at least 5 km. This disturbance existed in a region of southeasterly winds.

Figure 6c indicates two primary regions of systematic vertical motion: 1) a strong downdraft ($w \approx 2$ m s^{-1}) below 3 km over Senj and 2) a strong updraft ($w \approx 3$ m s^{-1}) just southwest of Senj, tilting northeast with height.

The cloud patterns for this day show up nicely in photographs (Plates 1–6) but are difficult to analyze quantitatively as the liquid water level is less than the instrument threshold (0.1 gm m^{-3}). The cloud boundaries shown in Fig. 6c are determined from the dewpoint depression. On the lowest upwind leg the aircraft skimmed the undulations in the cloud top, very near the upper boundary of the bora. In the descending air above Senj-Rab, dewpoint depressions of 14°C were reached. Further southwest, a well-defined cloud (Plates 2, 4 and 6) was present with strong updrafts on its northeastern edge. This cloud extended well above the upstream stratus deck. A mixing ratio analysis is not shown for this case as r is nearly constant (r = 1.5 to 3.2 gm kg^{-1}) except for points downstream near the sea surfaces where $r \approx 5$. This implies that the θ field was nearly identical with the θ_e field (not shown).

The turbulence encountered by the aircraft was restricted to a region downstream of the ridge, tilting northeastward with height (Fig. 6d). The strongest turbulence $\sigma_w^2 \approx 15$ m^2 s^{-2} was found at the lowest levels. All moderate and severe turbulence was found in clear air. Note that the turbulence roughly coincided with regions of systematic vertical motion. With brief aircraft penetrations through these regions, it was not possible to separate turbulence from small regions of steady vertical motion.

PLATE 5. View from P-3 (P307) at 1024 UTC at 44.73°N, 014.61°E. View is eastward towards the coast just south of Senj from an altitude of about 900 m. Note clearing by descent and white caps on the Adriatic Sea indicating strong winds. (Photo A. Walker)

PLATE 9. View from the P-3 (P415) at about 0900 UTC. View is northeastward towards the Yugoslavian coastal range. Note bora stratus clouds upwind of mountain crest. Whitecaps on the sea indicate strong winds. (Photo R. Smith)

PLATE 7. View from the Electra (E325) at about 1000 UTC. View is southward along the coast south of Senj. Southeastern tip of Krk is in lower right. Note two levels of wave cloud. This was the only ALPEX bora flight with NE flow above the NE bora, thus allowing vertical propagation of mountain waves. (Photo R. Smith)

PLATE 10. View from the P-3 (P415) at about 1000 UTC. View is northward along the coast north of Senj. Note turbulent lee cloud. (Photo R. Smith)

c. 22 March

This flight took place about 40 hours after the onset of bora (Fig. 3). It was a deep, dry bora with northeasterly flow extending to 3.7 km at Zagreb (Fig. 7a). The lower three aircraft legs lay inside the bora layer with the lowest leg finding a strong bora acceleration, from 20 kt (11 m s^{-1}) to 40 kt (22 m s^{-1}), beginning over Karlovac. The flow above the bora was generally northwesterly, roughly perpendicular to the section.

The potential temperature pattern (Fig. 7b) suggests that most of the stability in the incoming flow was concentrated in an inversion between 3 and 4 km. The lower parts of this inversion descended by more than 1 km while the upper parts descended less than 400 m. Kinematically, this resulted in a reduced stability downstream. Note that the isentropes were not simple streamlines because of the turbulence and shift in wind direction over Senj. The absence of clouds allows the use of water vapor mixing ratio as an alternative tracer. (Fig. 7c). The strong descent between 2 and 3 km is consistent with the isentropes in Fig. 7b. Systematic downward air motion was found over the ridge crest ($w \approx -2$ m s^{-1}) with ascent present just downstream ($w \approx +2$ m s^{-1}). No systematic vertical motions were found at the 3.3 and 3.9 km levels. Turbulence levels of $\sigma_w = 10$ m^2 s^{-2} were found at the lowest level (1.5 km) with weak turbulence still detectable at 3.3 km.

Further discussion of the 22 March case is given in section 4.

d. 25 March

This flight occurred on the last day of the bora period shown in Fig. 3. The supply of cold air was nearly zero as evidenced by the shallow weak inversion and low

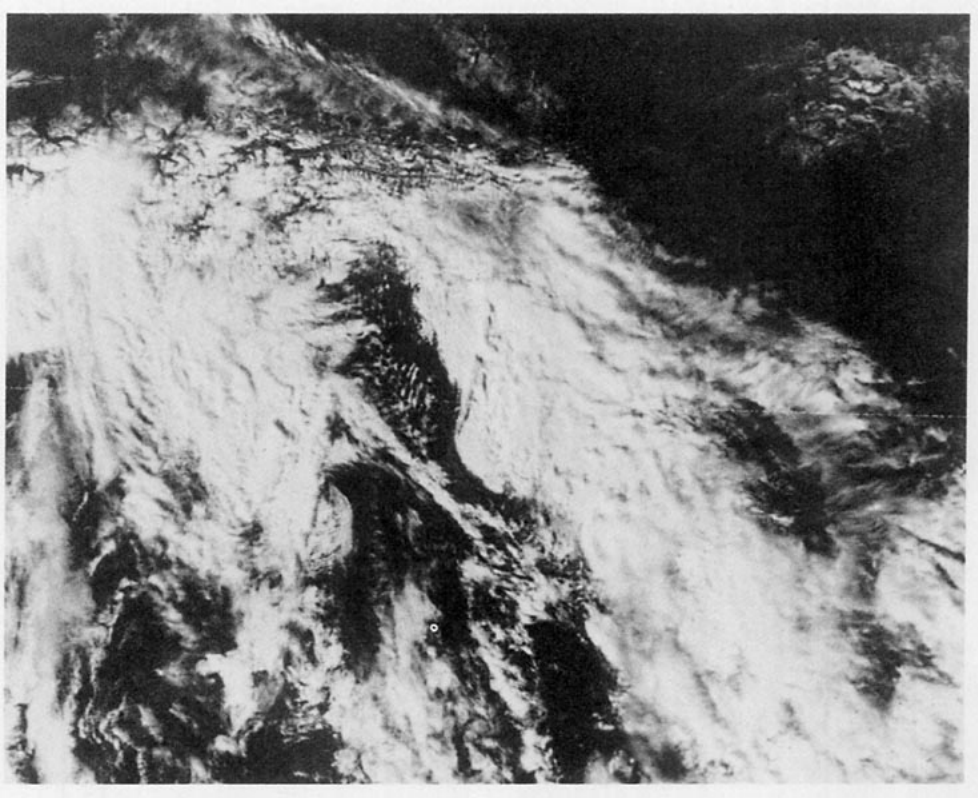

PLATE 6. Visible satellite image from polar orbiting satellite at 1310 UTC 7 March 1982. Boundary of bora stratus follows the Yugoslavian coastal range. North–south cloud line over Senj is probably turbulent lee cloud. It is not seen south of Pag in agreement with aircraft views (Plates 2 and 3). The inland extension of the cloud to the north is unexplained. (image from NESDIS)

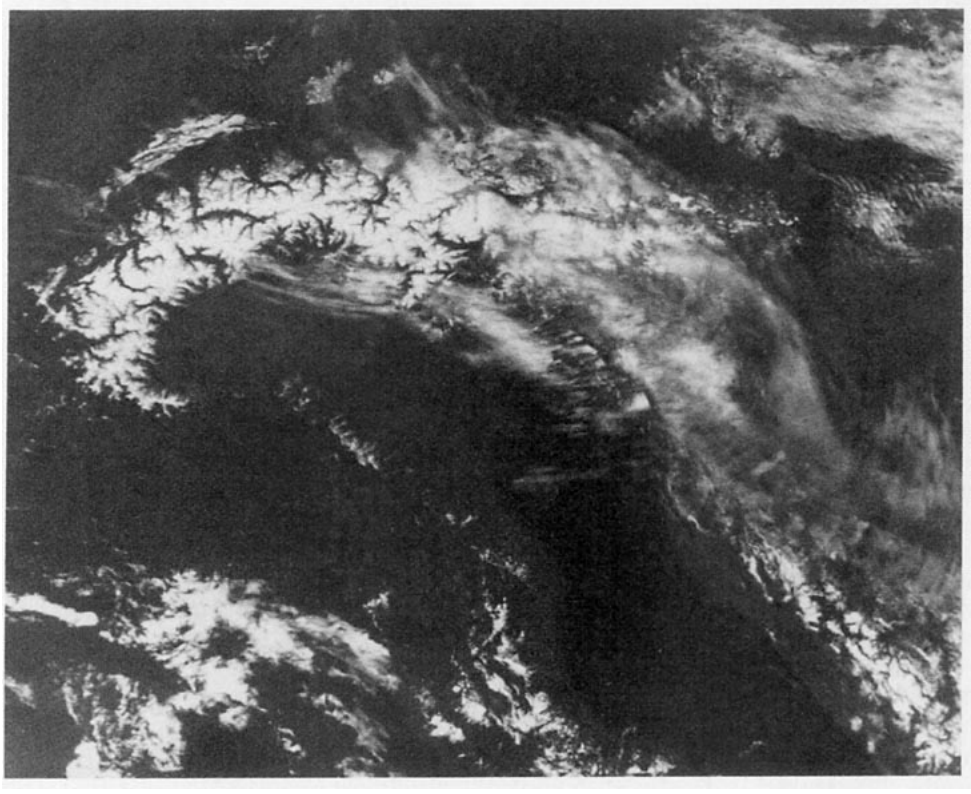

PLATE 8. Visible image from polar orbiting satellite showing the northern Adriatic at 1259 UTC 25 March 1982. Note middle or upper level wave cloud banners streaming westward from the Yugoslavian coastal range. All banners are north of Senj. (image from NESDIS)

wind speeds at Zagreb. The bora winds at Senj, however, were still moderately strong ($\sim$15 m s^{-1}).

This bora condition was unique among the five cases because of the small directional wind shear in the environment. The wind was northeasterly at all altitudes. This was qualitatively consistent with the observations of mid and upper level wave clouds (Plates 7, 8).

The flight data are limited by the lack of low level runs near the mountain (Fig. 8a). In addition, there was a rapid temporal increase in the humidity in the 650 mb to 500 mb layer which makes a steady state mixing ratio analysis unusable (not shown). The increased humidity allowed the formation of wave clouds which provided important visual clues to the nature of the flow.

The depth of the bora layer in this case is best estimated from the inversion in Fig. 8b at about 2 km. The detailed pattern of isentrope descent is not discernible, but from the aircraft sounding at 1033 UTC, some descent (approximately $-$700 m) and a weakening of the inversion was evident far downstream. The descent at Krk might have been much greater than this. Near the top of the inversion and further aloft, small but non-negligible isentrope disturbances were observed. These may have been connected with the observed wave clouds.

Light turbulence was found at 2.5 km (Fig. 8c) but this is possibly just the top of a more intense region below.

e. 15 April

This flight occurred during the third day of the bora period in Fig. 4. The supply of cold air had slackened considerably from the previous day, yet the bora was only slightly weaker. The winds aloft were from the south and southwest.

Two cross sections are presented in Figs. 9 and 10. The tracks from Zagreb toward Senj and toward Krk are shown in Fig. 1. The two cross sections look similar in many respects and will be described together. This similarity suggests that the flow is nearly two-dimensional in this region (but see section 4).

In Figs. 9a and 10a it is clear that the aircraft did not fly in the bora air upstream of the mountain; thus no direct observation of the upstream acceleration is available. Low level flights near Senj did penetrate slightly into the bora air and winds up to 40 kt (22 m s^{-1}) were recorded.

Upstream of the ridge the stability was concentrated into an inversion between 1.5 and 2.5 km. The environmental wind turning occurred through this stable layer. The lower part of the inversion descending strongly over Senj while the upper part, at about 2.4 km, was nearly undisturbed. This definition of bora depth nearly matched that from the environment wind shear (i.e., the depth at which Dir = 105°) in Figs. 9a and 10a.

Figures 9c and 10c illustrate the distribution of water vapor mixing ratio. A moisture maximum centered at 2.6 km included the upper part of the inversion. The strong descent of the r = 3 and 4 g kg^{-1} isolines was consistent with the isentrope descent. The moist layer lies primarily in southeasterly flow and thus was passing through the section, rather than flowing within it. Some upstream and downstream clouds are shown in Plates 9 and 10.

Intense turbulence was found at the lowest flight levels, over Senj. As before, it was not possible to separate turbulence from steady state jets in this inhomogeneous flow.

Further discussion of the 15 April case is given in section 4.

4. Three-dimensional bora structure

Two bora flights, P322 and P415, undertook extensive three-dimensional surveys in addition to the cross sections described in the previous section. Data from these legs are presented here in a series of maps, each with data taken close to a specified altitude. In this section, only horizontal wind and vertical turbulence are described. These map views should be examined together with the cross sections in section 3 to gain a full picture of the flow.

a. 22 March

Figure 11 illustrates the field of horizontal wind along three lines roughly parallel to the coastal range. The wind field at 2735 meters (Fig. 11a) shows the same upstream acceleration seen earlier in Fig. 7a. Along the line over the ridge, the air to the northwest had been accelerated to a speed similar to that in the Senj section (30 to 40 kt) but the flow to the southeast is much slower. This air either has not accelerated or has already decelerated. The Senj section is located very close to a region with different flow characteristics.

Farther southwest a second cross-line shows similar variation. The wind along the northwestern part of the line was slower than upstream as the bora layer had dropped below the line. The southeastern end had light and variable winds.

The wind field at 2140 m (Fig. 11b) shows more of an influence of the bora than the level above, with northeast winds prevailing. At 1215 m (Fig. 11c) the winds near Pula were stronger still as this was well within the bora layer even though it was quite far downstream from the coast ($\sim$80 km). At both lower levels, the bora appeared as a horizontal jet with its shearing boundary extending southwest from Rab or Pag.

The turbulence intensity along these same lines is shown in Fig. 12. Smooth flow was present upstream at 2735 m but turbulence was found at the southeast end of the first line. The significance of this is not clear. At 2140 m the strongest turbulence was located near

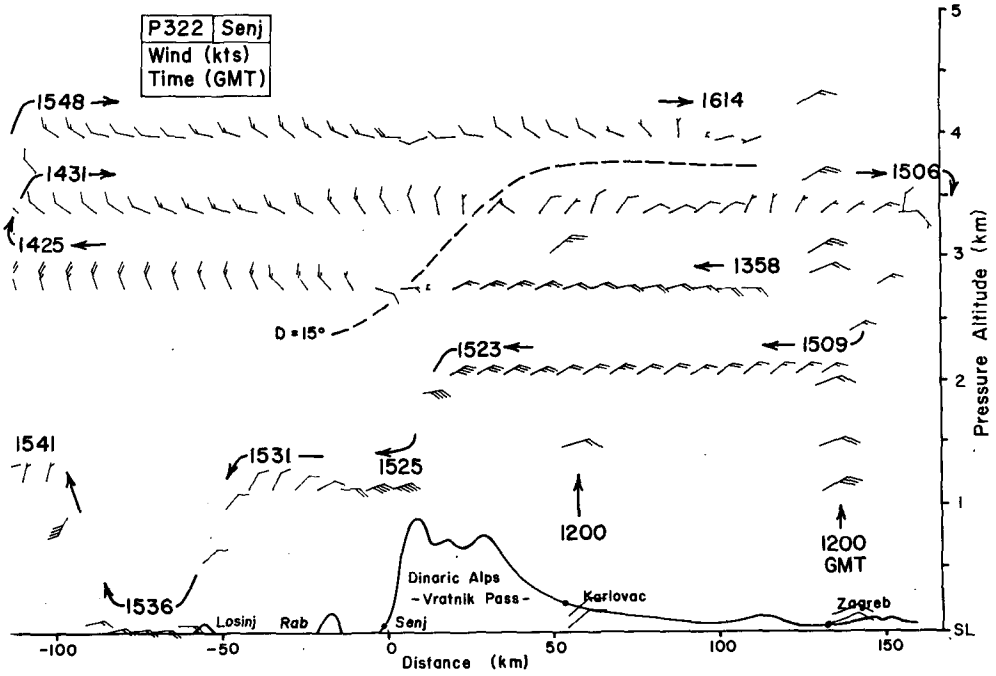

FIG. 7a. Wind cross section for mission P322. Dashed line (wind dir. = 15°) indicates where wind has turned 45° from the nominal bora wind direction (60°). Depth of bora allowed several flight legs within the NE airstream. At 2 km the wind accelerates from 15 kt (8 m s^{-1}) to 40 kt (22 m s^{-1}) upstream of the mountain crest.

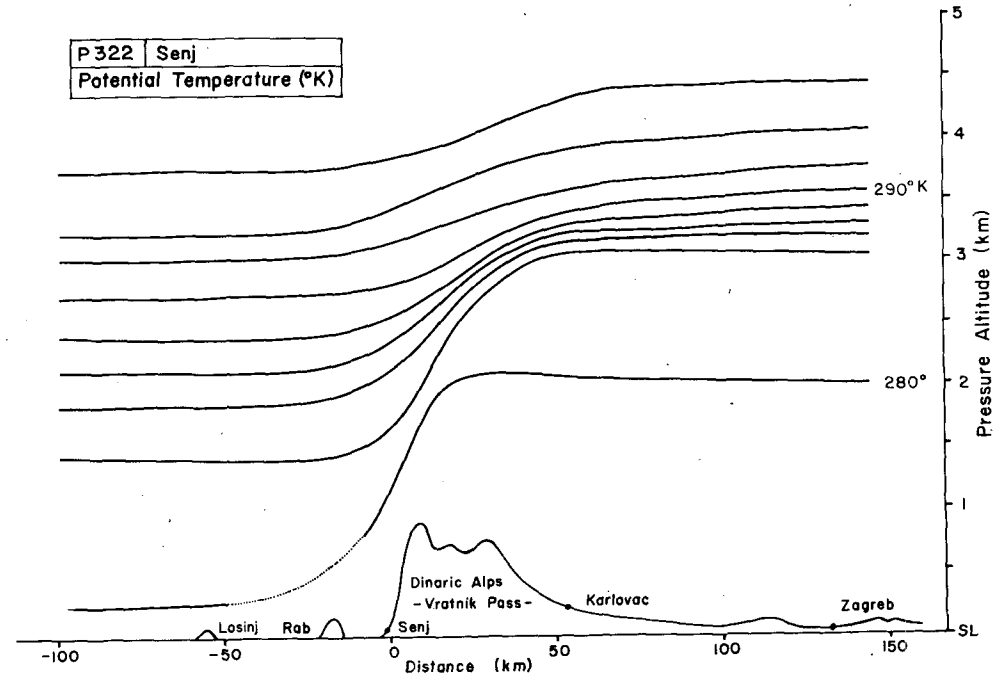

FIG. 7b. Potential temperature cross section for P322. Strong descent is evident below 0.5 km, beginning over Karlovac. Upstream inversion is weakened downstream.

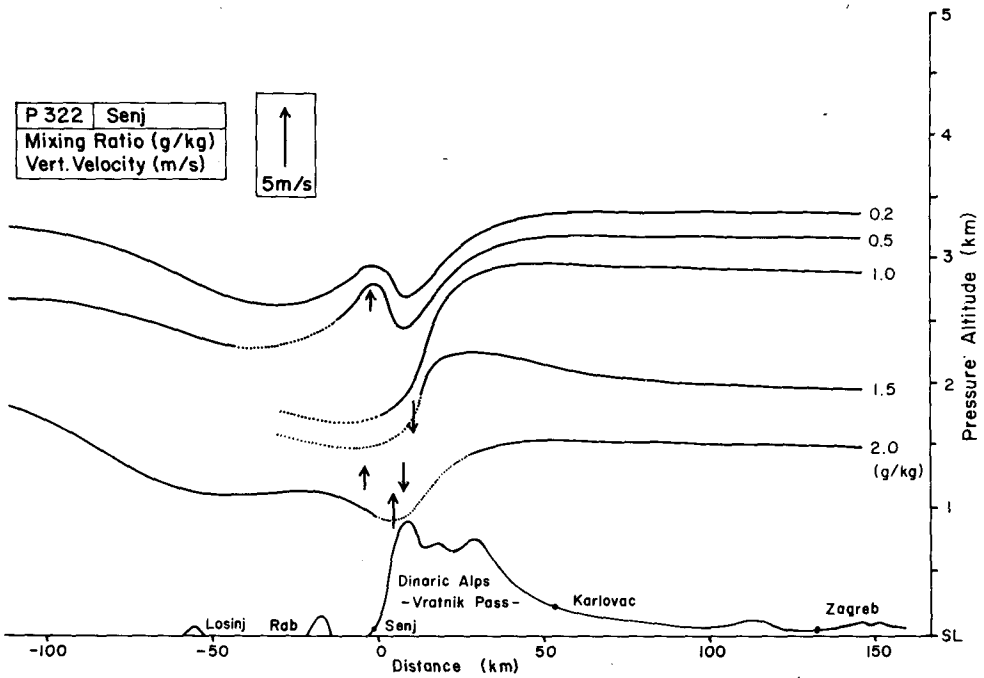

FIG. 7c. Water vapor mixing ratio cross section for P322. Contours of r roughly agree with θ (e.g., $r = 1.0$ g kg^{-1} and $\theta = 282°$K) in the bora layer but not when crossing the turbulent zone into the northwesterly air mass. Vertical velocity field indicates descent ($w \sim -2$ m s^{-1}) over ridge crest followed by ascent ($w \sim 2$ m s^{-1}) over Senj.

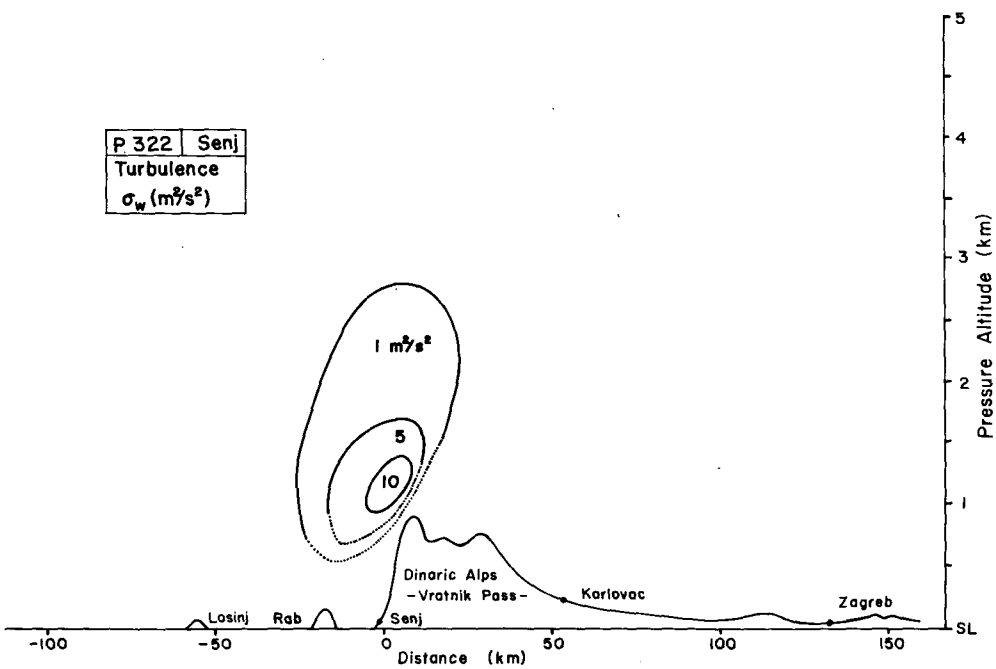

FIG. 7d. Turbulence cross section for P322.

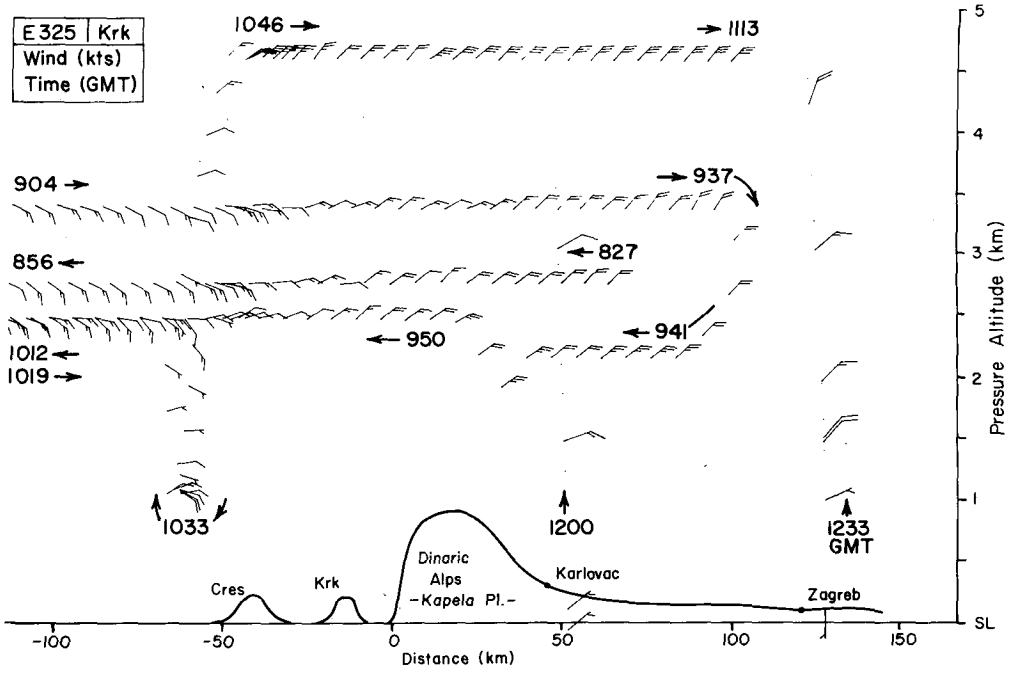

FIG. 8a. Wind data on the Krk cross section for mission E325. This is the only ALPEX bora mission without directional wind shear in the environment. Wind is NE at all levels. Aircraft is above bora layer (defined by the inversion) and no upstream acceleration is observed.

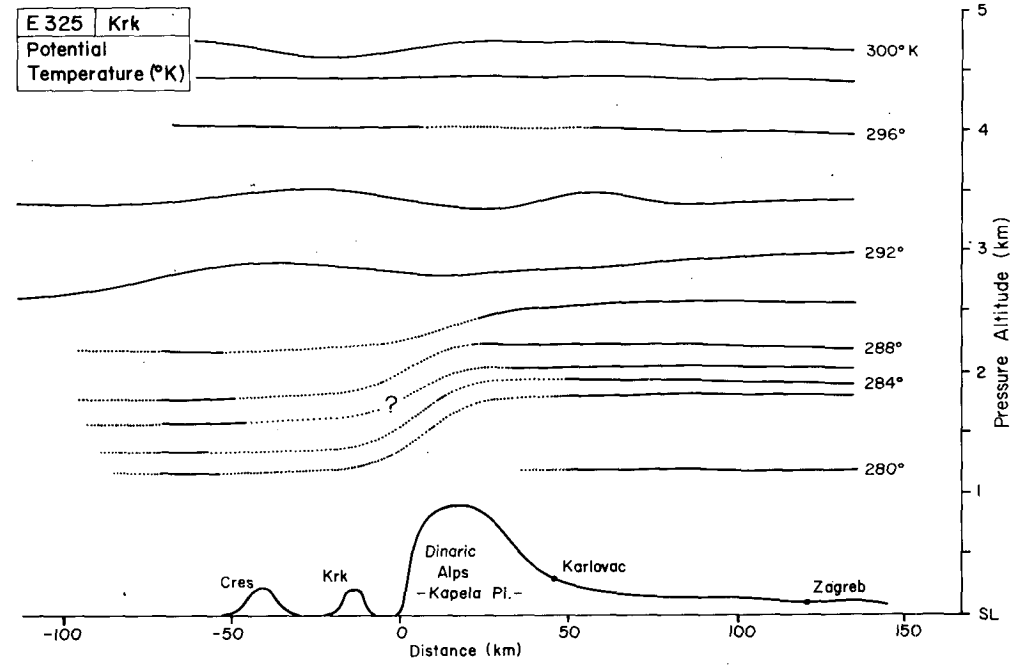

FIG. 8b. Potential temperature cross section for E325. Lack of low level aircraft data over Senj prevents analysis of the descent pattern. Inversion is less pronounced downstream. Slight isentrope displacement is evident aloft in agreement with wave clouds in Plates 7 and 8.

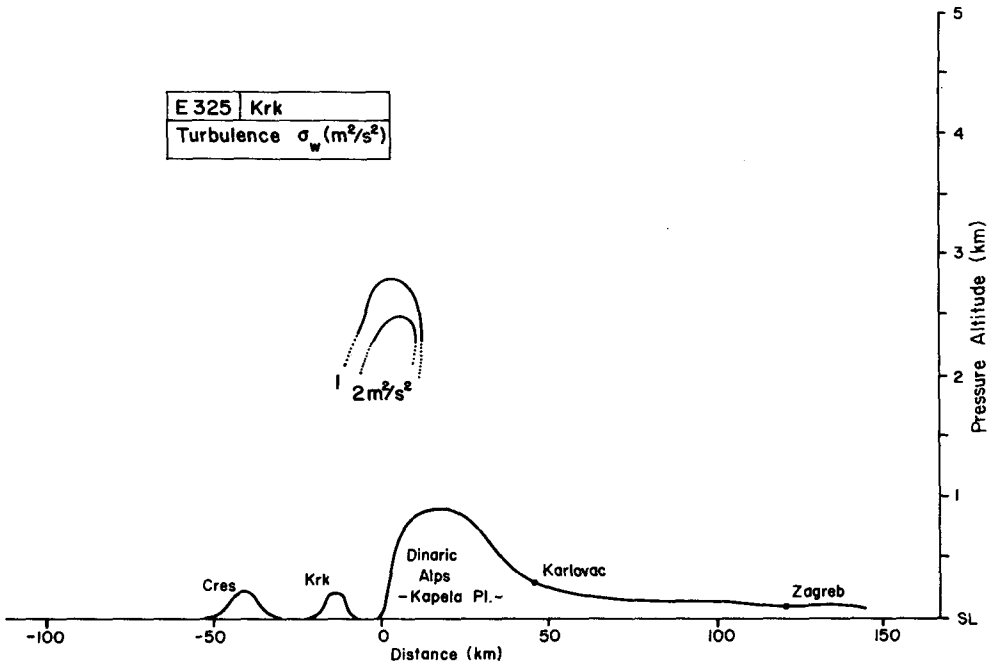

FIG. 8c. Turbulence cross section for E325. Only the upper part of turbulent zone is penetrated by the aircraft.

the coast. A spot of turbulence further southwest coincides with the shear line in the horizontal wind. At 1215, the flow was smooth except for light turbulence on the southwestward extending shear line.

b. 15 April

In addition to the two cross sections described in section 3, a four-level box pattern was flown on this day (Figs. 13 and 14). The highest legs (2150 m in Fig. 13a) were generally above the bora with southeasterly winds as discussed earlier. At lower altitudes (Figs. 13b, c, d) the winds turned more from the northeast and increased in strength. Even at the lowest altitude (880 m), the aircraft was in the shear zone above the bora, rather than being fully inside the bora layer.

The turbulence in the box pattern is shown in Fig. 14. Smooth air was present at 2150 m with turbulence intensity increasing below. The strongest turbulence was located close to the coast. Near Senj at 880 m, values of $\sigma_w^2 > 15$ m^2 s^{-2} were recorded.

5. Characteristics of bora turbulence

One of the most striking features of the bora is the region of turbulence revealed in the cross sections and the three-dimension flight patterns, each constructed from the 1 second aircraft dataset. Further analysis of this turbulence is possible as high frequency data is available from both the P-3 (40 Hz) and the Electra (20 Hz). With a nominal aircraft speed of 120 m s^{-1}, this allows a spatial resolution of 3 or 6 meters, respectively. We report here on an initial attempt to characterize bora turbulence by looking at periods of the highest intensity turbulence from three flights. These are summarized in Table 2. The location of each turbulence record can be found in the earlier figures using the times and altitudes provided. No attempt will be made to relate these observations to turbulence characteristics at the surface (e.g., Petkovsek 1984).

A salient characteristic of bora turbulence is its spatial inhomogeneity. The intensity and other properties are strongly dependent on the length and starting location of the chosen record. The maximum σ_w^2 values computed from 10 or 20 second records (Figs. 5d, 6d, 7d, 8c, 9d, 10d, 12 and 14) reach values nearly an order of magnitude greater than the σ_w^2 values computed from 100 to 400 second records (Table 2). This was true even when the aircraft flew along the coast, perpendicular to a reasonably two-dimensional airflow (i.e., Fig. 14). A related problem is the large difference between the statistical properties of raw data and the same record with the linear trend removed. In spite of this uncertainty we will comment on some important features.

The variances of the three wind components compare as follows (from Table 2)

$$\sigma_u^2 \approx \sigma_v^2 \approx R\sigma_w^2, \tag{1}$$

where $R = 3 \pm 1$ and where u, v, w are eastward, northward and upward. Thus, there was about six times as much turbulent kinetic energy in the horizontal as in the vertical. The ratio R can be compared with other types of turbulence. For neutral boundary layers on a rigid wall (Panofsky and Dutton 1984, p. 160)

$$\sigma_u^2 = 3.7\sigma_w^2, \quad \sigma_v^2 = 2.37\sigma_w^2 \tag{2}$$

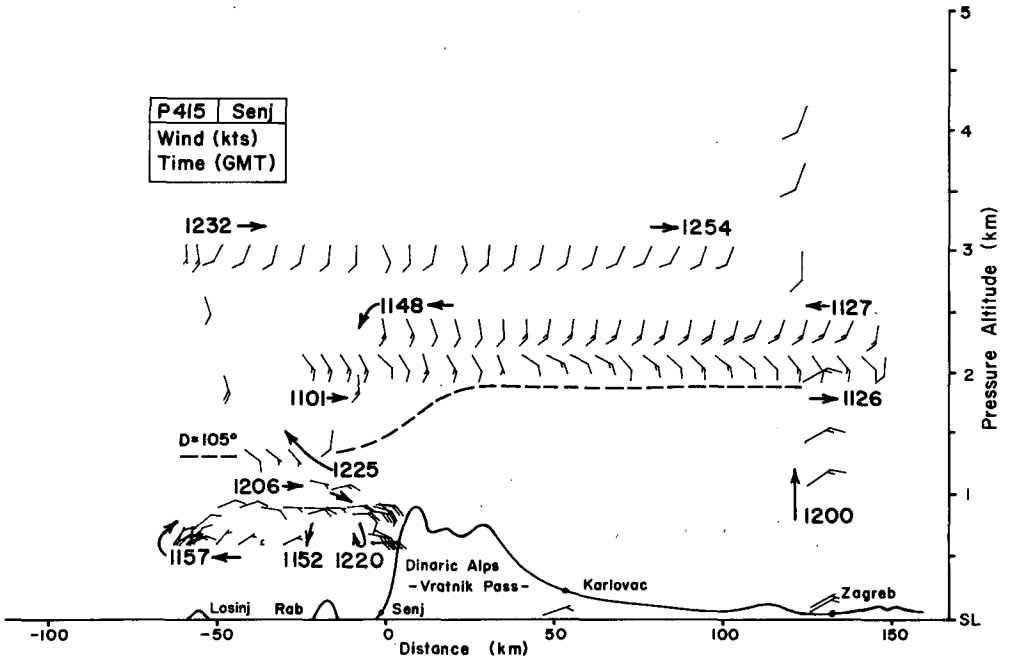

FIG. 9a. Wind data on the Senj cross section for mission P415. The shallow bora prevented aircraft penetration upstream of the ridge crest but strong winds are found over Senj. The dashed line (wind direction = 105°) marks the approximate upper boundary of the NE bora flow.

where u and v are downstream and crosstream components, and thus R again is about 3. In the presence of an upward/downward heat flux, σ_w will increase/decrease with height relative to σ_u and σ_v.

A more relevant comparison is with a free shear layer. Under neutral conditions in the laboratory (Wygnanski and Fiedler, 1970)

$$\sigma_u^2 = 1.44\sigma_w^2, \quad \sigma_v^2 = 0.87\sigma_w^2 \tag{3}$$

on the center line where u and v lie in the plane of the

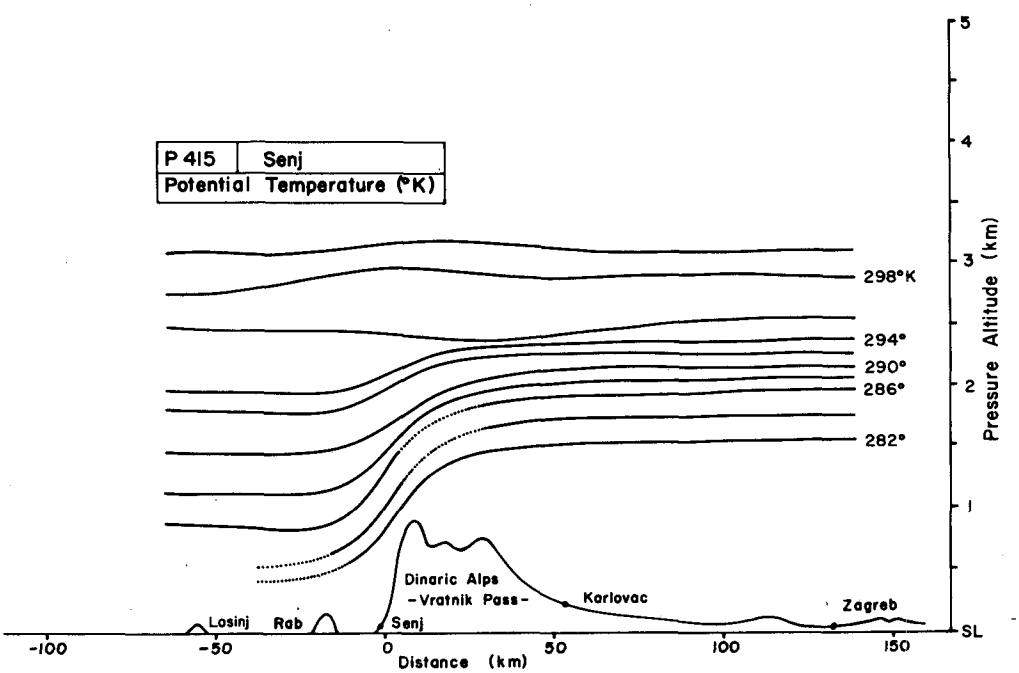

FIG. 9b. Potential temperature data on the Senj cross section for P415. Strong descent occurs below 2.5 km beginning over Karlovac. Upstream inversion is weakened and spread downstream.

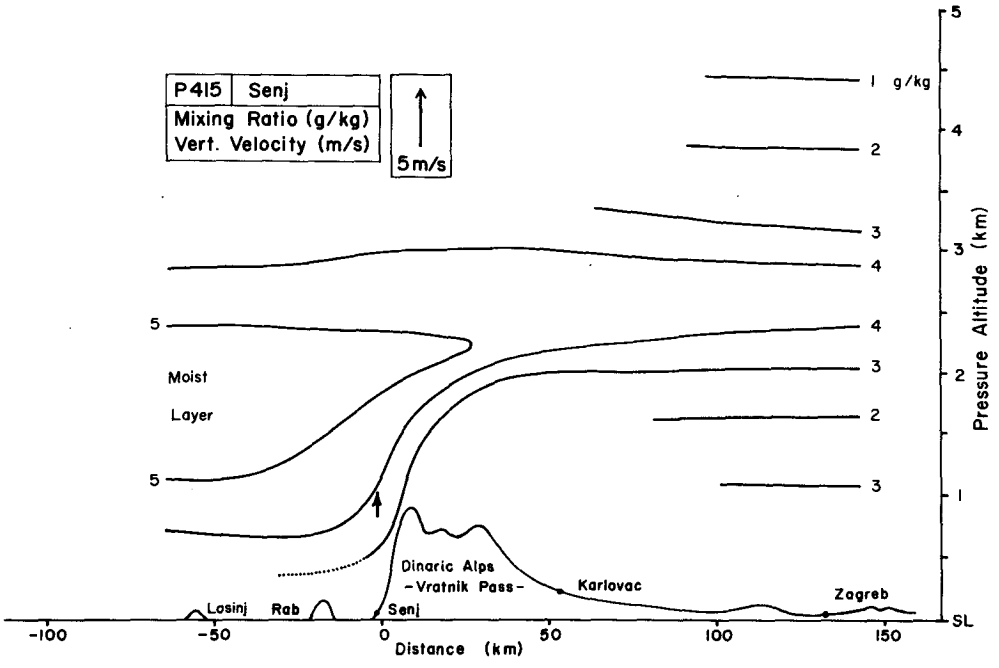

FIG. 9c. Water vapor mixing ratio on the Senj cross section for P415. Descent of the 3 g kg^{-1} contour from 2 km agrees with isentrope $\theta = 286$°K in Fig. 9b. The moist layer above lies in SE air (i.e., normal to cross section). Its thickness is modulated by the descent in the bora air below.

shear layer—u being the component parallel to the mean shear. As in (2), the slight dominance of σ_u^2 in (3) ($R \approx 1.3$) suggests a shear origin for the turbulence. The effect of stable stratification is small if the initial gradient Richardson number is small, but the effect increases as the mixing zone widens downstream. The vertical variance σ_w^2 decays more rapidly than σ_u^2 and σ_v^2 in this situation leading eventually to nearly two dimension turbulence; $R \to \infty$ (Koop and Browand, 1979).

A relevant atmospheric comparison is with the convective mixed layer with overlying inversion observed by Zhou et al. (1985). Values R = 3–4, 1–2, and 5–15 were found at increasing altitudes through the bound-

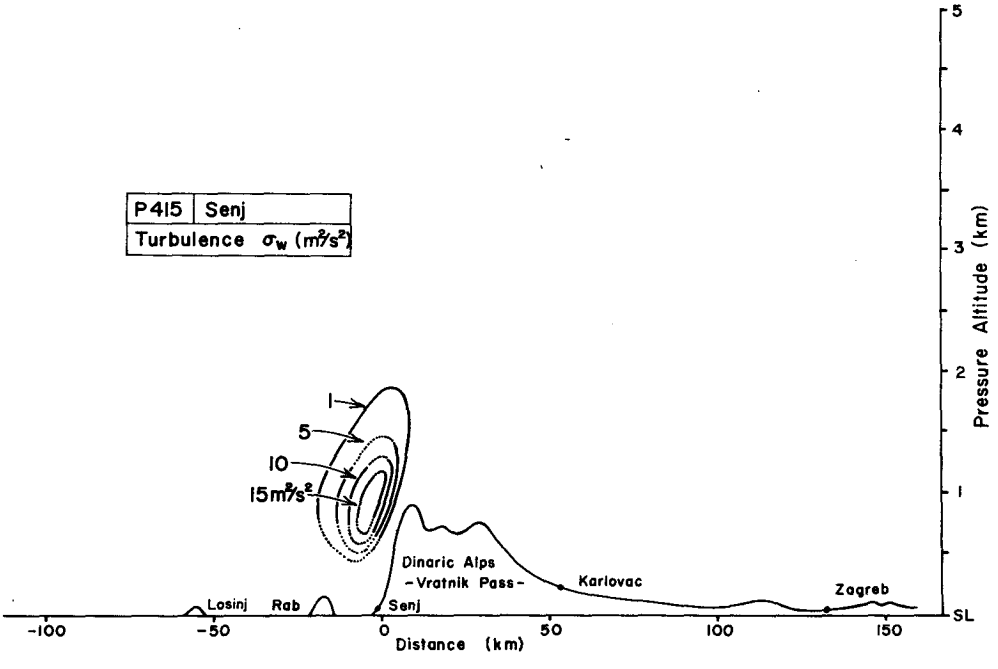

FIG. 9d. Turbulence in the Senj cross section for P415.

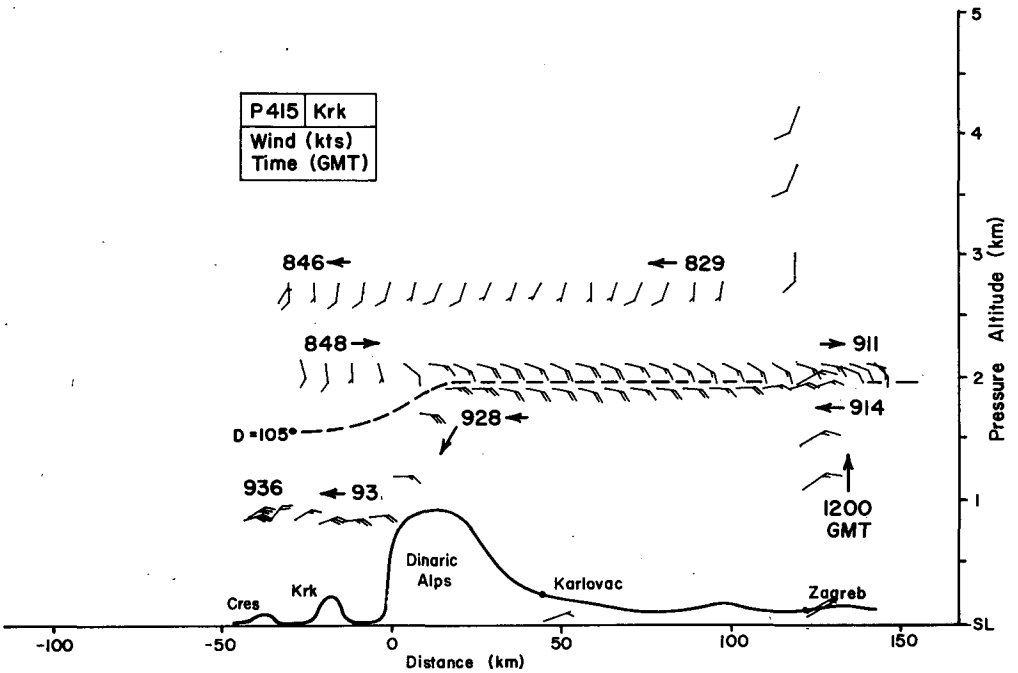

FIG. 10a. Wind data in the Krk cross section for P415. This section lies slightly north of the Senj section in Fig. 9. Wind field is similar to Fig. 9a but slight lower aircraft penetration upstream gives evidence of an airflow acceleration from 15 kt (8 m s^{-1}) to 25 kt (13 m s^{-1}).

ary layer. The first of these values is roughly consistent with (2), while the other values reflect the convective and stable conditions further aloft.

The covariance of vertical velocity and temperature is overwhelmingly negative in the examples of Table 2. A typical heat flux is -100 W m^{-2}. This is much too small a value to have appreciably heated the thick fast-moving bora layer but could have acted to heat or cool shallower slower layers with large flux convergence. A negative heat flux is consistent with the idea of shear induced mixing in a statically stable layer. It suggests that neither wave overturning nor mixing of

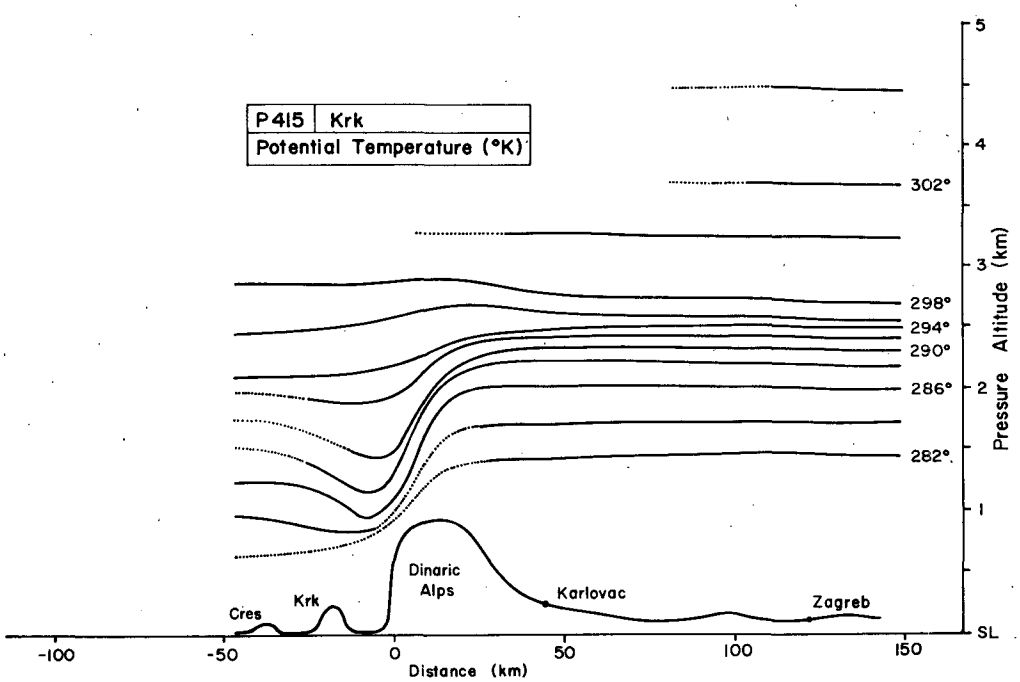

FIG. 10b. Like Fig. 9b but for the Krk section.

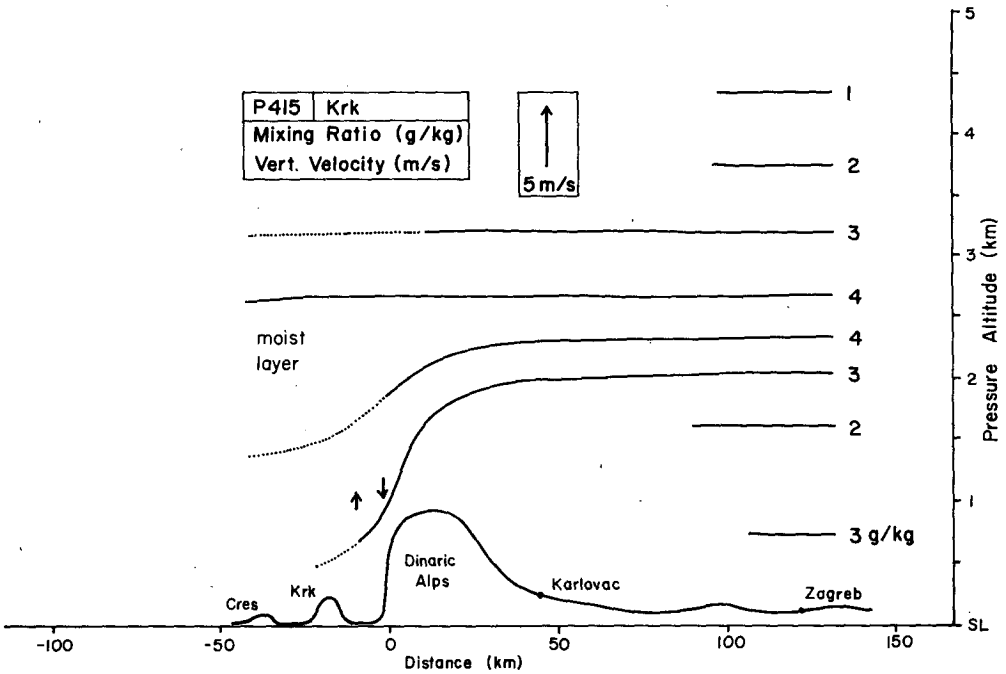

FIG. 10c. As in Fig. 9c but for the Krk section.

warm air upward from the marine layer over the Adriatic were dominant. The only strongly positive heat flux in Table 2 was from E306 (see also Mahrt, 1984). Possibly the proximity of dense cloud (Fig. 5c) may have allowed latent heat effects or errors from sensor wetting. More likely, the turbulence record includes the quasi-stationary cold descending bora and warmer upward jet (Figs. 5b, c) which comprise a positive heat flux.

The computed values of vertical transport of eastward and northward momentum show little systematic behavior. Simple downgradient momentum mixing above the northeasterly bora should give negative values for both of these quantities. On the other hand, the

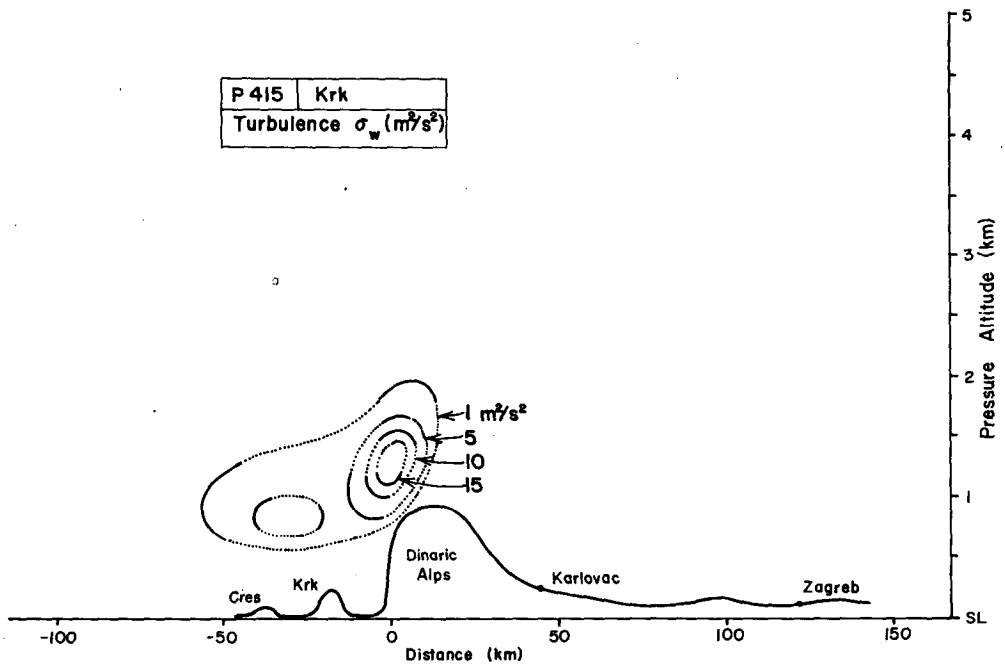

FIG. 10d. As in Fig. 9d but for the Krk section.

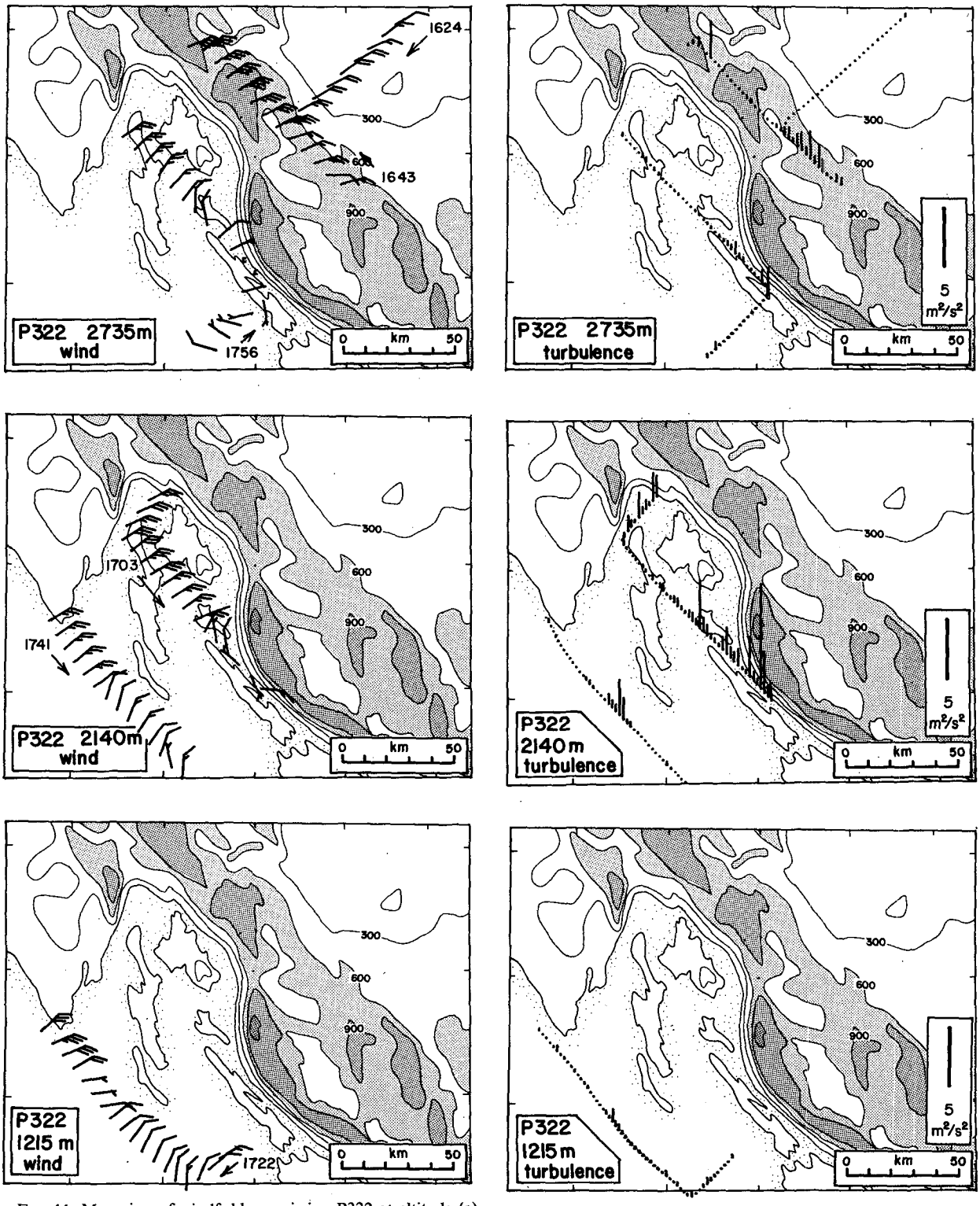

FIG. 11. Map view of windfield on mission P322 at altitude (a) 2735 meters above mean sea level; (b) 2140 m and (c) 1215 m. In (a) upstream acceleration on the Senj section seems representative of conditions to the northwest, but not to the southeast. Downstream of the ridge crest, stronger winds are found at lower altitudes (b) and (c). In (b) and (c) the Senj cross section line (see Fig. 1) also seems to be an approximate boundary between different wind regimes.

FIG. 12. As in Fig. 11 but for turbulence intensity. Length of vertical line is proportional to vertical wind variance over a 20 second interval without trend removal. Some turbulence is seen in (a) over the mountains SE of the Zagreb-Senj track. Stronger turbulence is seen at lower altitudes close to the lee slopes.

mean bora flow may try to bring southwestward momentum downward to be consistent with the large southwestward pressure drag on the mountain range. The variability of the computed momentum flux is probably another indication of the difficulty in separating mean flow and turbulence.

The downward heat flux, the anisotopy, and the location of the turbulence are consistent with the following picture. Under the sloping inversion over the mountain, the cold air accelerates and strong shear is generated at the top of the bora layer. Kelvin-Helmoltz instability leads to a shear-generated turbulent mixing region which deepens and weakens quickly downstream.

6. Summary of bora structure

Although the bora varies considerably in depth, in the strength of the incoming low level flow, and in the direction of the winds aloft, several common features are evident from the five bora cases. These include:

1) *Upstream acceleration.* On two days, 6 and 22 March, the aircraft was able to fly within the bora layer upstream and directly observe this acceleration. This acceleration was probably present in the shallower cases as well. The acceleration begins about where the mountains begin to rise (Karlovac) and continues as the air spills below the aircraft flight level. This observation contradicts the simplest model of a "fall wind"; that is, acceleration only when the air is moving downslope.

The observation of isentrope descent is consistent with the observed upstream acceleration in two ways. First, the conservation of mass flow rate between the rising terrain and the descending isentropes, would require flow acceleration. Second, the descending isentropes produce a horizontal density gradient which hydrostatically gives rise to a pressure gradient below. This pressure gradient is directly responsible for the flow acceleration. The observations from the five cases suggest that the isentrope descent begins where the terrain rises (i.e., Karlovac).

2) *The stagnant region downstream.* A common feature of all five cases was the region of low stability (isentrope spreading) downstream of the crest. This region seems to fill the gap between the descending bora air and less disturbed conditions aloft. The region has slow winds (in the plane of the cross-section) and its leading boundary is highly turbulent.

In the four cases with wind turning in the environment, the upper boundary of the region (where the isentrope deflection is small) nearly coincides with the height at which the environmental wind turns by 45° or more from the bora wind direction (60° from true N). Thus the isentropic layer or streamtube at this level splits with the upper branch remaining nearly level and the lower branch descending strongly.

The one case with no wind turning, 25 March, also exhibits isentrope splitting and spreading downstream. In all five cases the splitting streamline originates from the middle of the inversion upstream, with the result that only the lower part of the inversion descends and plays a role in bora acceleration. This observation agrees with laboratory simulations (not described here) and is relevant to the application of hydraulic theory and the computation of the Froude number (section 8).

3) *The turbulent region.* Every one of the five cases included a narrow zone of turbulence just downstream of the mountains. From the mean isentropic analysis through this region (statically stable) and the turbulent heat flux (downward), we conclude that the turbulence is shear driven. The turbulence is strongest at the lowest levels flown but may weaken near the surface in the main bora layer. The wind variance anistropy is too large to be explained by shear driving alone but requires a nearby boundary or mean static stability. The latter is the more likely candidate.

Two systematic regions of vertical velocity are imbedded in and partly included in the estimated turbulent region. The main bora downdraft is found whenever the aircraft is properly located. A sloping updraft just beyond the downdraft seems almost equally reliable, and is probably responsible for the observed lee-side "jump" or "rotor" cloud found in some cases.

4) *Three-dimensional effects.* The two flights with three-dimensional flight patterns reveal some common features. Both flights find a remarkable regime change just southeast of Senj. This is probably produced by the bend in the coastline and increased breadth of the range beyond this point. The line of demarcation (oriented NE–SW) can be traced from the first mountain ridge well out to sea where it marks a strong horizontal wind shear and associated turbulence.

5) *The bora environment.* Although the bora seems able to occur under a wide range of conditions, one condition seems necessary. There must be a supply of low level cold air from the east. Surprisingly, moderate bora can persist until this supply is nearly exhausted. The vertical distribution of stability seems not to be crucial. Strong sharp inversions (22 March) or more constant low level stability (6 and 7 March) will suffice. Wind turning or reversal aloft is a common but not an essential feature.

7. Bora in relation to other downslope winds

The similarity in the five bora cases (section 6) and their resemblance to the Boulder windstorm structure (Lilly and Zipser, 1972; Lilly, 1978), especially items 1–3 above, suggests that a variety of environmental conditions and terrain geometry can give rise to a nearly common final state. It is necessary, however, that each of these severe wind environments have some feature which prevents a simple pattern of vertically propagating or trapped waves. These simple wave patterns are well understood theoretically and often observed

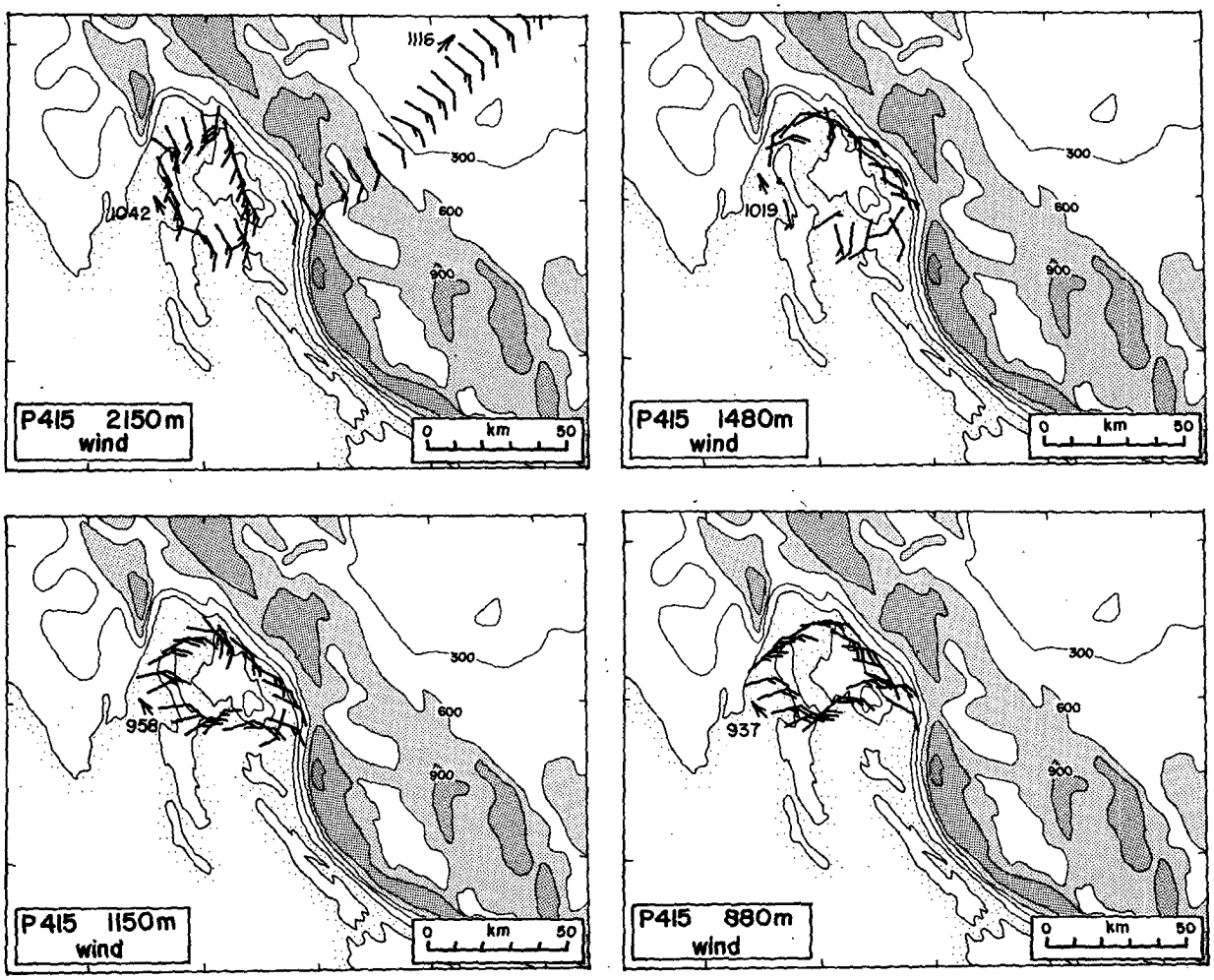

FIG. 13. Map view of wind field on mission P415 at altitude (a) 2150, (b) 1480 m, (c) 1150 m, (d) 880 m. The highest level, 2150 m, lies above the bora in the SE air. At 1480 and 1150 m, the wind is weak and transitional in direction. At 880 m the wind is stronger (≈20 kt, 11 m s^{-1}) with some component from the NE.

in the atmosphere (see the reviews by Alaka, 1960, and Smith, 1979) but they do not seem to offer a quantitative explanation for severe downslope winds. Two wave-destroying environmental features are recognized.

a. Large effective mountain height ($\hat{h} = hN/U$)

The idea that large $\hat{h}$ will generate wave breaking was probably understood by Queney (1948). Estimates of wave breaking altitudes were given by Huppert and Miles (1969) and Smith (1977). Evidence that breaking would lead to a severe wind state arose from numerical experiments by Clark and Peltier (1977, 1984) and unpublished laboratory experiments by A. Foldvik in the early 1970s (personal communication, 1976).

Unfortunately, it is not only $\hat{h}$ that determines if waves will break. Resonant reflection (Klemp and Lilly, 1975), or nonlinear effects arising from stability layering (Smith, 1976) can amplify mountain waves and promote earlier wave breaking.

The bora case of 25 March, the only case with NE winds at all levels, seems to illustrate this situation. The weak wind and strong layered stability give a large effective mountain height ($\hat{h}$) preventing a laminar mountain wave field. The Boulder windstorm of January 11, 1972 (Lilly and Zipser, 1972) seems to be another example in this class. The higher average windspeed over Boulder is counteracted by a greater mountain height (see Table 3) and perhaps other factors to prevent a simple mountain wave field.

b. Wind reversal

A case with small $\hat{h}$ may still lead to wave breaking aloft if the environmental wind component across the ridge drops to a small value or reverses at some altitude. If the mountain is very small and the "critical layer"

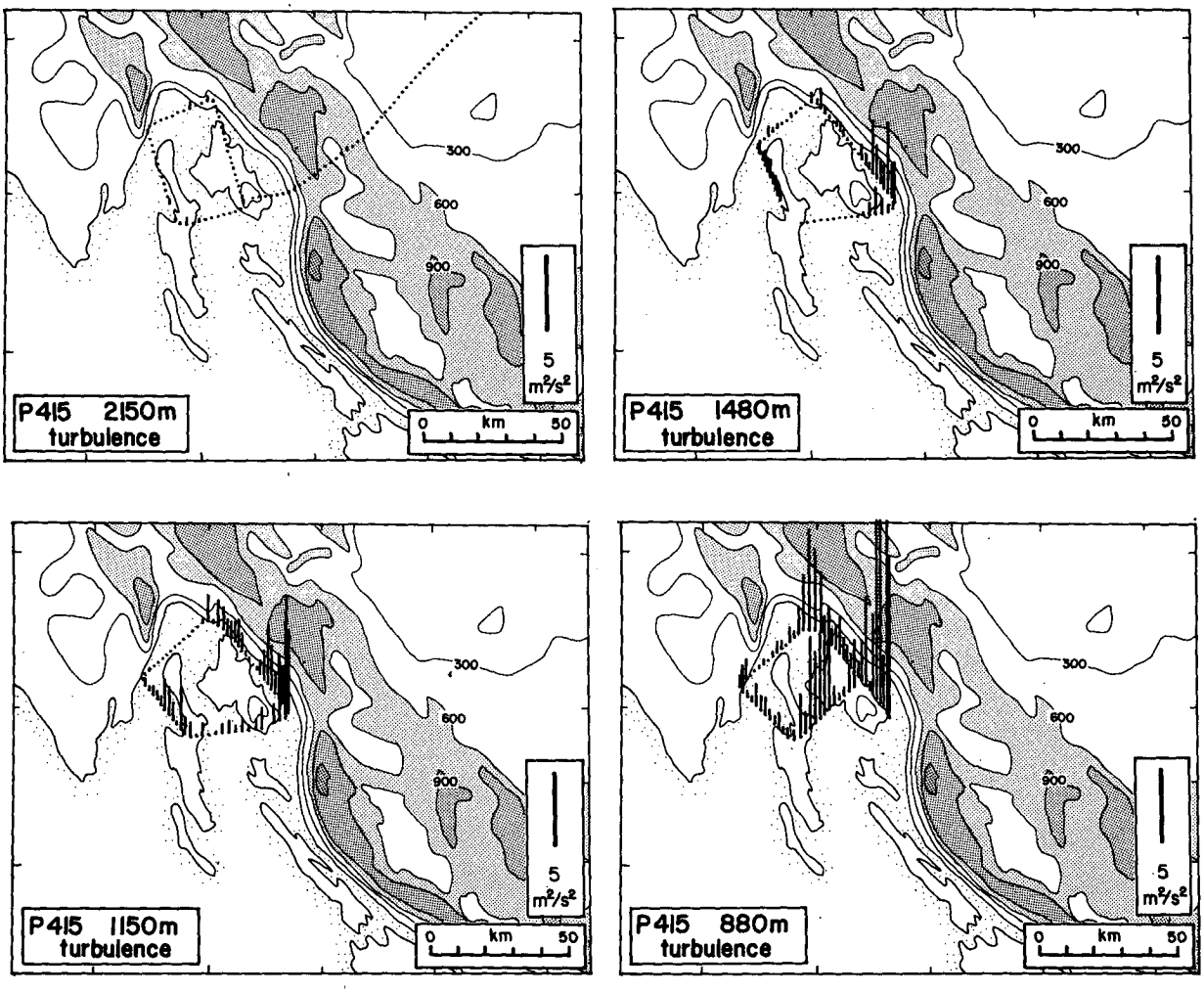

FIG. 14. As in Fig. 13 but for turbulence intensity. The highest level is free from turbulence. Turbulence is strongest at the lowest level flown and closest to the coast, especially near Senj.

dominated by viscosity, wave absorption will take place and a severe wind condition does not occur (Booker and Bretherton, 1967). In other conditions, a severe wind configuration is possible, as seen in the numerical calculations of Klemp and Lilly (1978) and Clark and Peltier (1984).

The effect of a wind reversal is relevant to the bora on 6, 7 and 22 March and 15 April. Vertically propagating waves are prevented by the turning of the winds to a direction normal to or reversed from the northeasterly bora flow. It may be that the wind speed and stability would give a large $\hat{h}$ and severe wind even without the wind reversal. Nevertheless, these cases represent a distinct class of flow because the wind turning was present and the bora structure developed to be consistent with it. The split streamline and turbulent region occur at heights which are consistent with the environmental wind reversal height upstream.

The wind reversal case may also be relevant to other windstorms such as the Windy Gap flow in Wyoming (Marwitz and Dawson, 1984). The shallow Alpine foehn may also have this character (Smith, 1986).

8. Application of hydraulic theory

We now turn our attention to the structure of the severe wind flow. The discussion in sections 6 and 7 indicates that severe wind flow fields have common features whether or not they are triggered by large $\hat{h}$ or by a wind reversal. We consider the applicability of "internal hydraulic theory" as a mathematical description of these common features (Smith, 1985).

Hydraulic theory, as used here, will refer to a nonlinear hydrostatic theory of fluid flow in which the upper boundary condition, usually a constant pressure head condition, renders the equations local. We take hydraulic theory to encompass any distribution of stability within the layer whether continuous (Smith,

TABLE 2. Turbulence characteristics.

Index	Flight	Start time (GMT)	Duration (sec)	Var (u)	Var (u^*)	Var (v)	Var (v^*)	Var (w)	Var (w^*)	Heat flux	Heat flux*	Momentum flux Fl.E.	Momentum flux Fl.*E	Momentum flux Fl.N	Momentum flux Fl.*N	Location	Altitude processed
1	E306	1331:06	180	19.4	11.9	77.8	5.6	6.3	6.2	+150	+540	+.4	+1.5	+.9	+1.5	Senj	2700 m G
2	E306	1449:06	180	27.8	16.3	58.0	13.3	12.1	11.6	+30	−220	—	—	−7.5	−6.0	Senj	2400 m G
3	P322	1525:55	136	6.2	4.9	8.5	5.9	3.3	3.2	−0.5	+40	+.09	−.1	−.04	+.3	Senj	1173 m G
4	P322	1409:20	161		2.7		2.4		.69		−72		−.07		−.13	Senj	2782 m N
5	P322	1440:30	301		.8		1.1		.26		−6.9		−.04		+.01	Senj	3391 m N
6	P322	1525:55	321		4.8		5.3		1.6		+20		−.12		−.33	Senj	1173 m N
7	P322	1644:06	346		8.4		3.5		.93		−123		+.39		+.12	SEcrest	2772 m N
8	P322	1700:20	166		1.8		1.1		1.1		−49		+.35		+.23	Ncoast	2157 m N
9	P322	1709:30	451		16.2		3.1		1.7		−4.6		+.5		+.08	SEcoast	2158 m N
10	P322	1804:10	441		2.1		2.3		0.9		−208		+.02		−.04	offshore	2784 m N
11	P322	1811:35	226		1.2		1.7		0.3		−361		+.07		−.02	offshore	2785 m N
12	P415	0950:00	95	27.9	19.3	10.8	8.0	7.7	2.7	−150	−260	−.5	+.5	+2.0	+2.5	coast	880 m G
13	P415	1011:00	115	9.9	9.9	9.1	7.2	6.1	2.5	−310	−180	+3.0	+3.1	+.7	+.2	coast	1130 m G
14	P415	1032:00	100	6.2	6.0	3.3	3.2	3.1	3.1	−100	−100	−.2	−.2	−.3	−.3	coast	1480 m G
15	P415	1214:00	61	11.9	11.5	9.5	9.3	7.0	6.8	−670	−720	+1.5	+1.3	+3.7	+3.5	Senj	800 m G
16	P415	1220:00	159	22.0	14.0	10.7	4.7	4.9	4.8	−18	−230	+.4	+1.4	−.2	+.8	Senj	800 m G
17	P415	0932:05	116		8.3		4.4		3.8		−160		+1.8		−.3	Senj	897 m N
18	P415	0936:25	176		3.2		2.4		1.3		−33		+.15		+.4	Losinj	903 m N
19	P415	0946:15	321		12.3		4.1		3.5		−123		+.61		+1.0	coast	915 m N
20	P415	1007:30	326		7.2		3.6		3.0		−116		+1.3		−.3	coast	1223 m N
21	P415	1028:35	306		3.8		2.4		1.6		−16		−.35		−.13	coast	1523 m N

Notes: * linear trend removed from time series, G processed with NCAR Genpro software, N processed by NOAA, u, v, w are velocity components directed eastward, northward, and upward respectively, Momentum Flux N. = cov (v, w): Momentum Flux E. = cov (u, w) units: $m^2\ s^{-2}$, Heat flux = ρc_p cov (w, T) units: $W\ m^{-2}$, ($\rho \approx 1$ kg m^{-3}, $c_p = 1004$ J/kg°C)

1985), or interfacial (Long, 1954). Both types of stratification distribution are represented in our sample of five bora cases.

Qualitatively, the application of hydraulic theory is successful in a number of ways. The concept of transition from subcritical to supercritical flow offers an explanation of the upstream acceleration followed by further acceleration as the terrain drops. The concept of the mountain as a control point helps to understand how the flow can maintain its severe state as the upstream supply of cold air diminishes. The localness of hydraulic theory is consistent with the observed beginning of the disturbance where the terrain begins to rise. The strength of the acceleration is better explained by hydraulics than mountain wave theory, as mountain waves always have part of their accelerating pressure gradient cancelled by reverse density gradients aloft.

The constant pressure head condition, required in hydraulic theory, can occur in two ways. First, the fluid aloft may be nearly homogeneous so that vertical motions do not generate density anomalies (Long, 1954). Second, with mixing, there may exist an intermediate layer which fills in between the upper and lower layers, thus allowing the upper layer to be disturbance free (Smith, 1985). On this issue the evidence is strongly in favor of the second option. The Boulder windstorm, Windy Gap airflow and the five bora cases all show the turbulent intermediate layer with less disturbed stratified air aloft.

According to hydraulic theory, a certain relationship must exist between upstream wind, depth, and stratification, and mountain height, whenever the airflow accelerates over the ridge crest. For single layer flow this is given by

$$\frac{h}{H_0} = 1 + \frac{1}{2}F_0^2 - \frac{3}{2}F_0^{2/3} \tag{4}$$

from Long, 1954, where $F_0 = U\left[g\frac{\Delta\theta}{\theta}H_0\right]^{-1/2}$ and h and H_0 are the mountain height and upstream depth, respectively. For continuous stratification

$$\hat{H}_0 = \hat{h} - \hat{\delta} + \arccos(\hat{h}/\hat{\delta}) \tag{5}$$

where

$$\hat{\delta} = -\frac{1}{\sqrt{2}}[\hat{h}^2 + \hat{h}\sqrt{\hat{h}^2+4}]^{1/2}$$

and $\hat{H}_0 = H_0N/U$ and $\hat{h} = hN/U$ from Smith and Sun (1986). These two relations (4) and (5) are plotted in Figs. 15a and 15b. Points corresponding to the five bora cases and two other downslope winds (Lilly and Zipser, 1972; Marwitz and Dawson, 1984) are included. Cases with a neutral layer capped by an inversion are plotted in Fig. 15a, while cases with nearly constant stratification are plotted in Fig. 15b. Cases with stability profiles between the layered and continuous type (i.e.

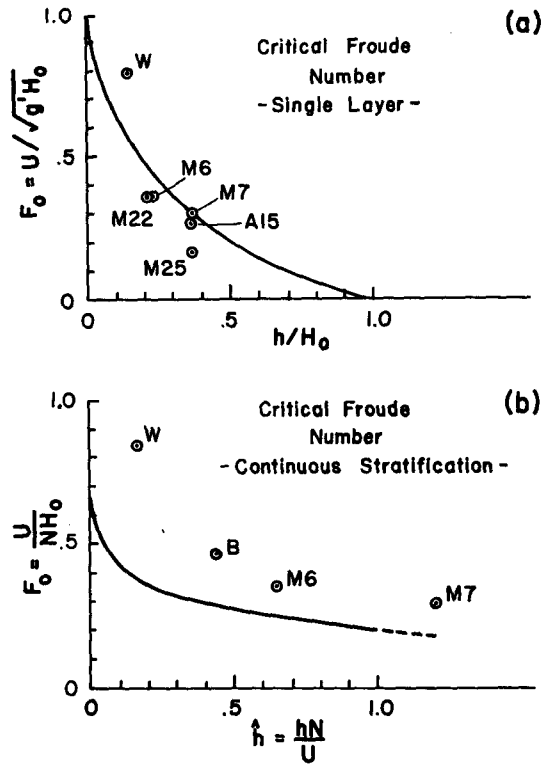

FIG. 15. A comparison of upstream conditions with the prediction of hydraulic theory under critical conditions. Part (a) is for a sharply defined stable layer (Eq. 4) while (b) is for uniform stability (Eq. 5). Five bora cases M6, M7, M22, M25 and A15, are shown, along with the 11 January 1972 Boulder windstorm (B) and 1 December 1976 Windy Gap, Wyoming, windstorm (W). Data is from Table 3.

M6, M7, and Windy Gap) are shown on both diagrams. Data used in locating these points are shown in Table 3. The overall agreement with theory is reasonably good, considering the numerous complicating factors in the real atmosphere such as variable wind and stability profiles, three-dimensional effects, the turbulent boundary layer, clouds, etc.

Two ideas follow from the agreement in Fig. 15. First, the hydraulic equation (4) or (5) provides a constraint that the local steady flow must satisfy. For the cases with a wind reversal, this probably requires that the mountain control the nature of the flow upstream. This is so because 1) we find agreement between the aircraft observations of the split isentrope and the upstream wind reversal and 2) it is not likely that the agreement shown in Fig. 15 is fortuitous.

For the cases without a wind reversal (the bora on 25 March or the Boulder windstorm) upstream control is still possible, especially if the upstream inversion has a definite top with nearly neutral conditions aloft. On the other hand, there may be nothing obvious in the upstream profile which indicates how deep the accelerating bora layer will be. In this case the flow may locally select the altitude of the split isentrope in order

TABLE 3. Hydraulic parameters.

Date	θ_{crit}[a] (°K)	Layered cases: h (m)	$\Delta\theta$ (°C)	H_0 (m)	U (m s^{-1})	F_0[c]	$\frac{h}{H_0}$
M6	292	800	16	3500	16	.36	.23
M7	288	800	14	2200	10	.3	.36
M22	290	800	10	3600	13	.36	.22
M25	288	800	8	2200	4	.16	.36
A15	290	800	8	2200	7	.28	.36
Windy gap	294	100	9	700	12	.8	.15
		Continuous cases				F_0[d]	$\hat{h}=\frac{hN}{U}$
M6	292	800	16	3500	16	.36	.65
M7	288	800	14	2200	10	.30	1.2
Boulder (1/11/72)	327.5	1600	25	9500	40	.48	.45
Windy gap (12/1/76)	294	100[b]	9	700	12	.85	.17

[a] Top of the descending layer.

[b] This small rise may not be the dominant control. Friction or 3-D effects may enter.

[c] $F_0 = U\left(g\frac{\Delta\theta}{\theta}H_0\right)^{-1/2}$

[d] $F_0 = U/NH_0$

to satisfy the hydraulic constraints. No upstream control is necessary.

The second implication of Fig. 15 is that the five bora cases and other downslope winds may have a common dynamical basis. They form a regular pattern of points in parameter space.

Some difficulties with hydraulic theory are as follows: first, the steady state nature of the theory prevents it from describing the evolution to or the stability of the final severe state; second, the theory suggests a relationship between environment and the height and thickness of the mixed region, but does not indicate how this adjustment occurs. Even when a fairly well-defined upstream inversion exists, one must not assume that it defines a hydraulic layer. It may be split with only the lower part involved in the hydraulic flow.

9. Conclusion

We have used recently acquired aircraft data in a comparative study of the bora. Several common features were apparent in the five cases considered (see section 6). The results indicate an internal hydraulic mechanism for the bora, with the mountains partially controlling the flow upstream and a turbulent layer helping to decouple the descending layer from the less disturbed flow aloft. The data supports neither the theory of vertically propagating waves nor the pure fall wind as the mechanism of the bora. The similarity between the different cases of Yugoslavian bora and severe downslope winds in other lands, both with regard to structure and nondimensional parameters, suggest a new unity to the subject.

Acknowledgments. The author is indebted to the ALPEX scientists, flight crews, and ground personnel who made the bora research flights possible. The analysis of the data was done with the assistance of Mark Bradford, Paul Gluhosky, Thomas Milnes, Steven Rivers, and Linn Stanton. Jie-Lun Sun assisted with some auxilary laboratory experiments. Useful comments on the manuscript were provided by Fedor Mesinger and Larry Mahrt. This work was supported by the National Science Foundation and the National Oceanic and Atmospheric Administration under Grant ATM-8306702.

REFERENCES

Alaka, M. A., 1960: The airflow over mountains, WMO Tech. Note 34, World Meteorological Organization, Geneva.

Booker, J. R., and F. P. Bretherton, 1967: The critical layer for internal gravity waves in a shear flow. *J. Fluid Mech.*, **27**, 513–539.

Clark, T. L., and W. R. Peltier, 1977: On the evolution and stability of finite amplitude mountain waves. *J. Atmos. Sci.*, **34**, 1715–1730.

——, and ——, 1984: Critical level reflection and the resonant growth of nonlinear mountain waves. *J. Atmos. Sci.*, **41**, 3122–3134.

Huppert, H. E., and J. W. Miles, 1969: Lee waves in a stratified flow, Part 3. Semi-elliptical obstacle. *J. Fluid Mech.*, **35**, 481–496.

Jurčeč, V., 1981: On mesoscale characteristics of bora conditions in Yugoslavia. *Pure Appl. Geophys.*, **119**, 640–657.

——, 1984: Strong bora case in Zadar and upstream bora layer characteristics. *Zbornik, Meteor. Hidrol. Radova,* **10,** 105–108.

Klemp, J. B., and D. K. Lilly, 1975: The dynamics of wave-induced downslope winds. *J. Atmos. Sci.*, **32,** 320–339.

——, and ——, 1978: Numerical simulation of hydrostatic mountain waves. *J. Atmos. Sci.*, **35,** 78–107.

Koop, C. G., and F. K. Browand, 1979: Instability and turbulence in a stratified fluid with shear, Part 1. *J. Fluid Mech.*, **93,** 135–159.

Koracin, D., 1984: Parameters of bora flow. *Zbornik, Meteor. Hidrol. Radova,* **10,** 109–111.

Lilly, D. K., 1978: A severe downslope windstorm and aircraft turbulence event induced by a mountain wave. *J. Atmos. Sci.*, **35,** 59–77.

——, and E. J. Zipser, 1972: The front range windstorm of 11 January 1972—a meteorological narrative. *Weatherwise,* **25**(2), 56–63.

Long, R. R., 1954: Some aspects of the flow of stratified fluids, II, experiments with a two fluid system. *Tellus,* **6,** 97–115.

Mahrt, L., 1984: Turbulence over the coastal range of northern Yugoslavia. *Zbornik, Meteor. Hidrol. Radova,* **12,** 46–49.

Marwitz, J. D., and P. J. Dawson, 1984: Low-level airflow in southern Wyoming during wintertime. *Mon. Wea. Rev.*, **112,** 1246–1262.

Panofsky, H. A., and J. A. Dutton, 1984: *Atmospheric Turbulence,* Wiley and Sons, 397 pp.

Petkovsek, Z., 1984: Some characteristics of bora gusts. *Zbornik, Meteor. Hidrol. Radova,* **10,** 245–248.

Queney, Paul, 1948: The problem of air flow over mountains: a summary of theoretical studies. *Bull. Amer. Meteor. Soc.*, **29,** 16–26.

Reed, R. J., 1981: A case study of a Bora-like windstorm in Western Washington. *Mon. Wea. Rev.*, **109,** 2382–2393.

Smith, R. B., 1976: The generation of lee waves by the Blue Ridge. *J. Atmos. Sci.*, **33,** 507–519.

——, 1977: The steepening of hydrostatic mountain waves. *J. Atmos. Sci.*, **34,** 1634–1654.

——, 1979: The influence of mountains on the atmosphere. *Advances in Geophysics,* Vol. 21, Academic Press, 87–230.

——, 1982: Aerial observations of the Yugoslavian bora: preliminary results, In ALPEX: Preliminary Scientific Results, World Meteorological Org. ALPEX Vol. 7, Geneva, Switzerland.

——, 1984: Aerial observations of the Yugoslavian bora. *Zbornik, Meteor. Hidrol. Radova,* **10,** 127–129.

——, 1985: On severe downslope winds. *J. Atmos. Sci.*, **42,** 2598–2603.

——, 1986: Mesoscale mountain meteorology in the Alps, *Proc. of the Venice ALPEX Conf.: October 1985,* WMO, Geneva.

——, and J. Sun, 1986: Generalized hydraulic solutions relevant to severe downslope winds, submitted to the *J. Atmos. Sci.*

Vucetic, V., 1984: On the time and space variations of the northern Adriatic bora. *Zbornik, Meteor. Hidrol. Radova,* **10,** 134–137.

Wygnanski, I., and H. E. Fiedler, 1970: The two-dimensional mixing region. *J. Fluid Mech.*, **41,** 327–361.

Yoshino, M. M., 1976: Local wind bora, University of Tokyo Press, 289 pp.

Zhou, M. Y., D. H. Lenschow, B. B. Stankov, J. C. Kaimal and J. E. Gaynor, 1985: Wave and turbulence structure in a shallow baroclinic convective boundary layer and overlying inversion. *J. Atmos. Sci.*, **42,** 47–57.